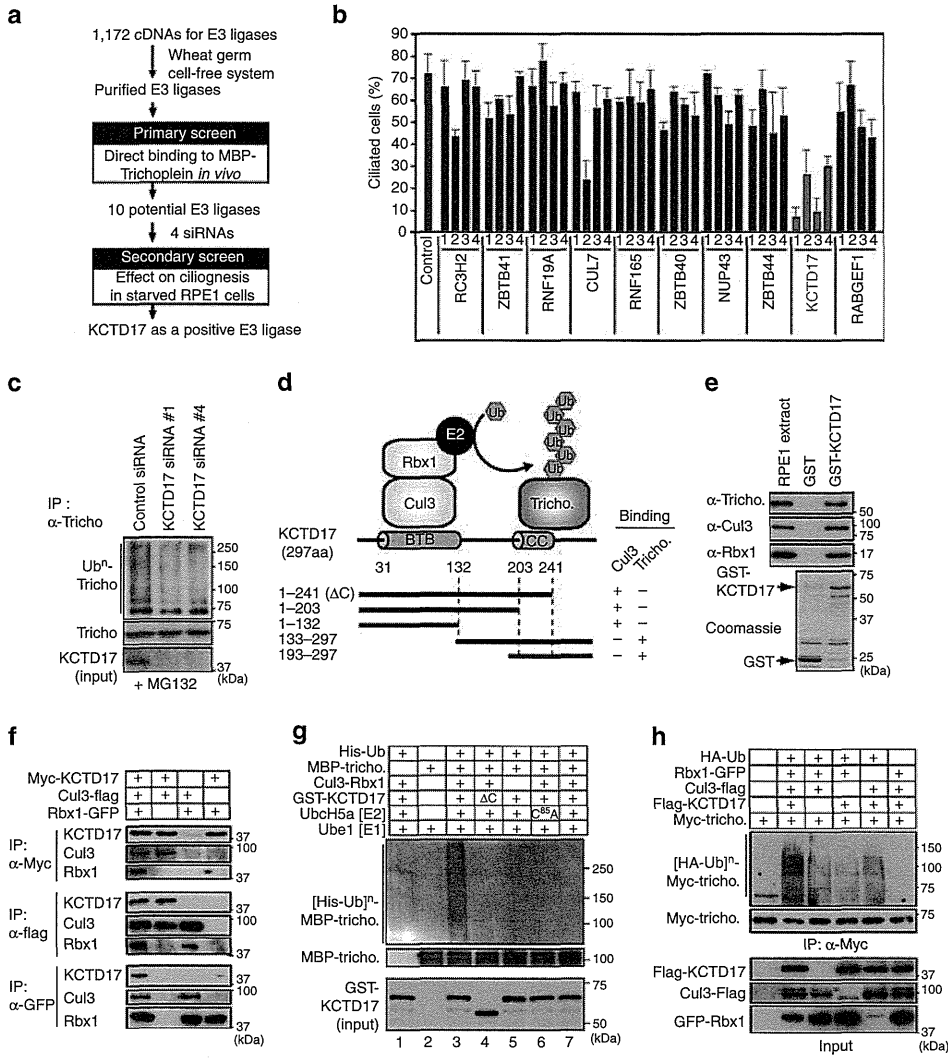

Figure 3 | CRL3-KCTD17 polyubiquitylates trichoplein. (**a**) A flowchart of two-stepped global E3 screen. (**b**) RPE1 cells transfected with four distinct siRNAs for indicated genes. 24 h after transfection, cells were subjected to 24 h serum starvation and percentages of ciliated cells were evaluated (mean ± s.e.m. from three indicated experiments, $n > 100$ each). (**c**) *In vivo* ubiquitylation assays of endogenous trichoplein in control or KCTD17-depleted RPE1 cells subjected to 6 h serum starvation in the presence of MG132. (**d**) Model for CRL3-KCTD17-mediated trichoplein polyubiquitylation (top). Schematic representative of KCTD17 fragments; interactions with Cul3 and trichoplein are shown by a plus sign and a lack of interaction by a minus sign (bottom). (**e**) Pull-down assays of trichoplein, Cul3 and Rbx1 with bacterially purified GST-KCTD17 from RPE1 cell extract. (**f**) Co-immunoprecipitation assays show interactions among Myc-KCTD17, Cul3-Flag and Rbx1-GFP in HEK293T cells. (**g**) *In vitro* ubiquitylation assays of MBP-trichoplein in the presence of indicated proteins. ΔC indicates GST-KCTD17 1–241aa fragment. $C^{85}A$ indicates catalytically inactive UbcH5a mutant. (**h**) *In vivo* ubiquitylation assays of Myc-trichoplein in HEK293T cells transfected with indicated cDNA. CC, coiled-coil; IP, immunoprecipitation.

starvation-induced ciliogenesis both in RPE1 cells and IMR-90 fibroblasts (Fig. 3b and Supplementary Fig. 4). Immunofluoresence analyses of cell cycle markers, including cyclin A and BrdU incorporation, exclude the possibility that the defective ciliogenesis is due to the inappropriate cell cycle re-entry (Supplementary Fig. 5). In addition, KCTD17 silencing attenuated the serum starvation-induced polyubiquitylation of trichoplein (Fig. 3c). Thus, KCTD17 is a novel regulator of ciliogenesis that involves in trichoplein polyubiquitylation.

CRL3-KCTD17 and UbcH5a/b polyubiquitylate trichoplein. KCTD17 interacted with trichoplein (residues 39–65aa) through its coiled-coil-containing carboxyl-terminal region (residues 193–297aa; Fig. 3d and Supplementary Fig. 6). To examine the mechanism by which KCTD17 modulates polyubiquitylation of trichoplein, we explored the other components of the KCTD17-containing E3 ligase complex. Pull-down and co-immunoprecipitation assays revealed that KCTD17 bound to Cul3, which serves as a scaffold for CRL3s[40–43], and that this interaction was mediated via its BTB (broad complex, tramtrack, 'bric-a-brac') domain (residues 31–132aa; Fig. 3d,e and Supplementary Fig. 6). KCTD17, Cul3 and a RING protein Rbx1/Roc1 were co-immunoprecipitated with each other (Fig. 3f), indicating that they are in the same complex.

As similar to KCTD17 loss, siRNA-mediated depletions of Cul3 and Rbx1 also interfered with the serum starvation-induced ciliogenesis both in RPE1 and IMR-90 cells (Supplementary Fig. 7), we reasoned that the ternary complex should function as an E3 ligase that polyubiquitylates trichoplein. To test this

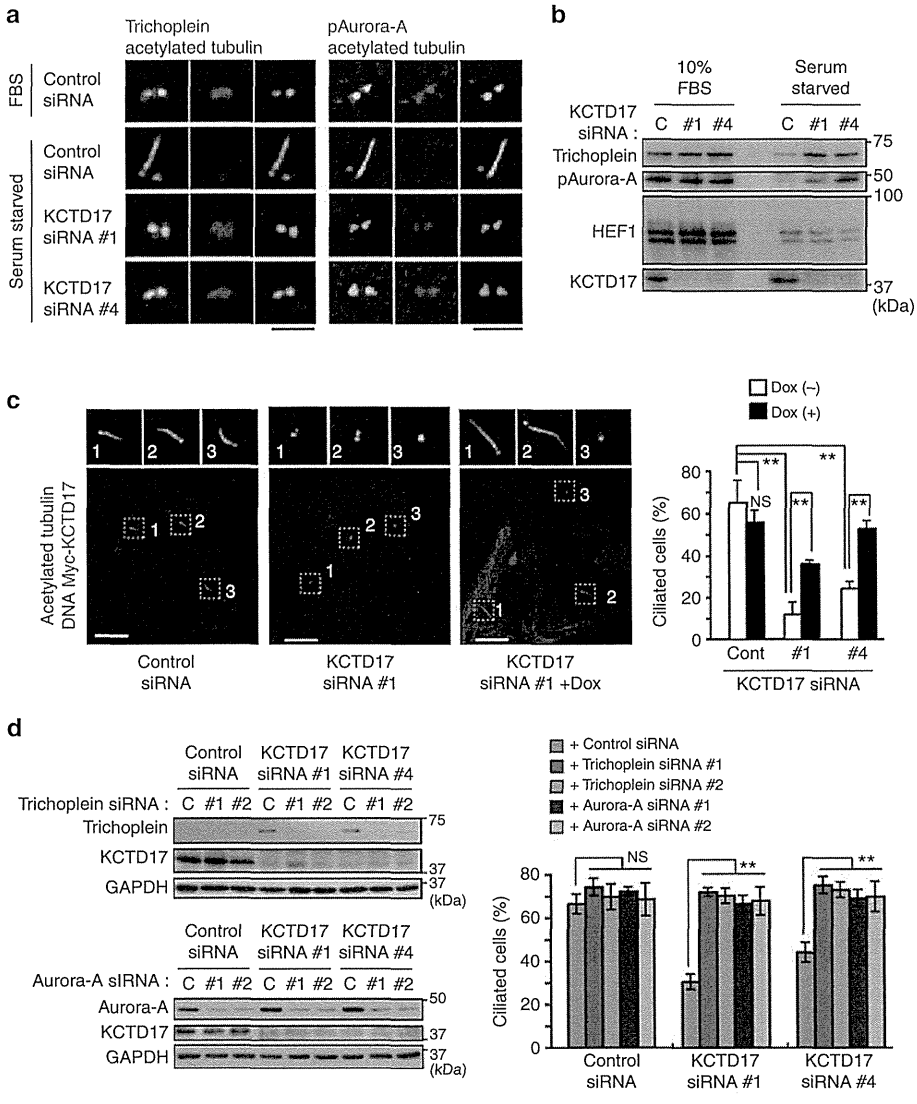

Figure 4 | KCTD17 downregulates trichoplein-Aurora-A pathway to promote ciliogenesis. (**a**,**b**) Effects of control or KCTD17 depletion (KCTD17 siRNA #1 or #4) on trichoplein-Aurora-A pathway in RPE1 cells cultured in normal medium (10% fetal bovine serum (FBS)) or subjected to 24 h serum starvation. Representative confocal images of trichoplein or pAurora-A (red) with cilia marker acetylated tubulin (green) are shown in **a**. Immunoblotting analysis of trichoplein, pAurora-A, HEF1 and glyceraldehyde 3-phosphate dehydrogenase (GAPDH) are shown in **b**. (**c**) Dox-dependent expression of myc-KCTD17 reverses the defect of serum starvation-induced ciliogenesis in KCTD17-depleted (#1 and #4) Tet-On RPE1 cells. Left, representative confocal images of acetylated tubulin (green), myc-KCTD17 (red) and DNA (blue) are shown. Right, percentages of ciliated cells (mean ± s.e.m. from three independent experiment, $n > 200$ each) are shown. (**d**) SiRNA-mediated silencing of Aurora-A (#1 and #2) or trichoplein (#1 and #2) reverses the defect of serum starvation-induced ciliogenesis in KCTD17-depleted (#1 and #4) RPE1 cells. Left, immunoblotting analysis shows levels of Aurora-A, trichoplein, KCTD17 and GAPDH. Right, percentages of ciliated cells (mean ± s.e.m. from three independent experiment, $n > 200$ each) are shown. $P^{**} < 0.01$, NS, not significant, two-tailed unpaired Student's *t*-tests. Scale bars indicate 2 μm (**a**) or 10 μm (**c**), respectively.

hypothesis, we performed *in vitro* reconstitution assays using bacterially purified ubiquitin, trichoplein, KCTD17, E1 (Ube1) and respective E2 enzymes, and Cul3-Rbx1 complex purified from HEK293T cells (Fig. 3g and Supplementary Fig. 8). Trichoplein was polyubiquitylated only when all of them were existed in reaction buffer (Fig. 3g; lane 3). KCTD17–trichoplein interaction is essential for the polyubiquitylation because a KCTD17 mutant (ΔC; 1-241aa) that could bind Cul3 but not trichoplein was insufficient (Fig. 3g; lane 4). Among E2s[44] we tested, UbcH5a and UbcH5b catalyzed *in vitro* polyubiquitylation of trichoplein (Fig. 3g; lane 6 and Supplementary Fig. 8). We further found that trichoplein was most efficiently polyubiquitylated in HEK293T cells when exogenous KCTD17, Cul3 and Rbx1 were co-expressed (Fig. 3h). Taken together, KCTD17 serves as a substrate-adaptor for CRL3 that polyubiquitylates trichoplein (Fig. 3d).

KCTD17 controls ciliogenesis via trichoplein and Aurora-A. As noted above, serum starvation caused the trichoplein removal from mother centriole through its proteolysis in control RPE1 cells, but these were prevented in KCTD17-depleted cells (Fig. 4a,b). KCTD17 silencing also disrupted the serum starvation-induced inactivation of centriolar Aurora-A (Fig. 4a,b), as trichoplein is a centriolar activator of Aurora-A[29]. Expression of siRNA-resistant myc-KCTD17 rescued all these phenotypes

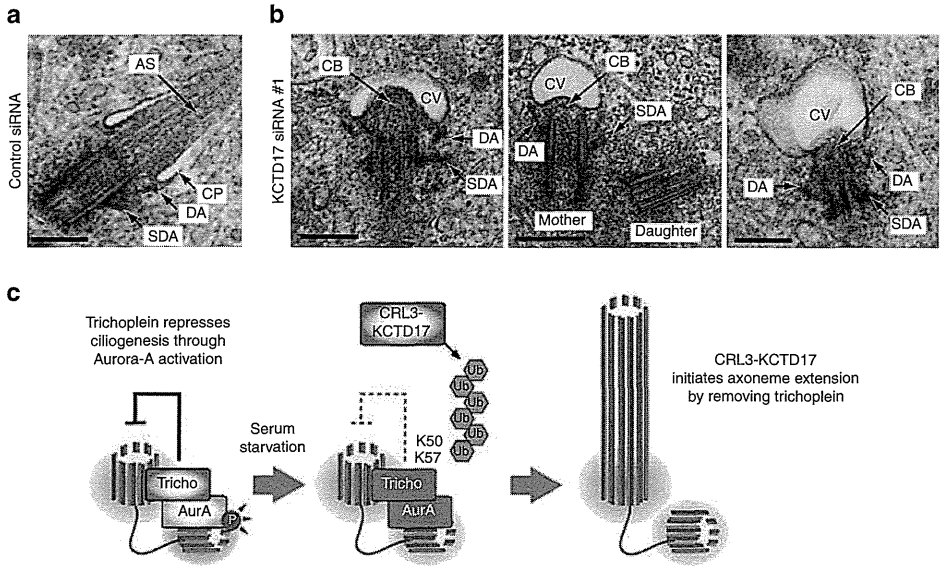

Figure 5 | KCTD17 depletion blocks axonemal extension during ciliogenesis. (**a**,**b**) Transmission electron micrographs of mother centrioles (single sections) in PRE1 cells transfected with control (**a**) or KCTD17 siRNA #1 (**b**), followed by 24 h serum starvation for ciliogenesis. AS, axonemal shaft; CB, ciliary bud; CP, ciliary pocket; CV, ciliary vesicle; DA, distal appendages; SDA, subdistal appendages. Scale bars indicate 500 nm. (**c**) Proposed model.

caused by KCTD17 depletion, namely the defective ciliogenesis (Fig. 4c) and the deregulated trichoplein-Aurora-A pathway (Supplementary Fig. 9). Similar results were also obtained in MBP-trichoplein-expressing Tet-On RPE1 cells (Fig. 2h,i; compare WT and WT + KCTD17 siRNA). HEF-1 is also reported to regulate ciliary dynamics by activating Aurora-A[24,33], but its protein levels were unchanged by KCTD17 depletion (Fig. 4b). These results indicate that KCTD17 contributes to trichoplein degradation and thereby inactivates Aurora-A to induce ciliogenesis.

It has been shown that trichoplein has numerous binding proteins other than Aurora-A[28,30] and its overexpression causes the mitochondrial fragmentation in some tumour cells[31,32] (see also Introduction). We found little changes in their protein levels (Supplementary Fig. 10) and the mitochondrial morphology (Supplementary Fig.11) by overexpression, depletion or stabilization of trichoplein in RPE1 cells under our experimental conditions, suggesting that trichoplein may have the cell type-specific functions. Furthermore, the defective ciliogenesis caused by KCTD17 depletion was completely reversed by co-silencing of trichoplein or Aurora-A (Fig. 4d). Thus, we propose that the KCTD17-trichoplein-Aurora-A pathway controls ciliogenesis in RPE1 cells.

KCTD17 depletion blocks extension of ciliary axoneme. To get more insight how KCTD17 regulates ciliogenesis, we analyzed mother centrioles and ciliary structures of serum-starved RPE1 cells lacking KCTD17 by transmission electron microscopy. Ciliogenesis follows a series of stereotyped steps that begin with the docking of CVs to the distal appendages of mother centrioles, followed by the formation and extension of ciliary axoneme[5,6] (Supplementary Fig. 12a). After 24 h serum starvation, control cells often demonstrated the mother centrioles that were associated with the ciliary pockets with extended axonemal shafts (Fig. 5a). In contrast, as approximately 90% of KCTD17-depleted cells lacked the elongated ciliary axoneme (see Fig. 3b; KCTD17 siRNA #1), in most of these cells (12 out of 16), the CVs efficiently docked to the mother centrioles, judged by the appearance of appendages, and became invaginated by the accumulated electron-dense materials at the distal end of centrioles (named the ciliary buds; Fig. 5b and Supplementary Fig. 12b). No gross alteration was detected in the ultrastructure of mother centriole. We therefore conclude that KCTD17 is not required for the maturation of mother centriole and the centriole-to-membrane docking, but instead, plays a crucial role in the initial step of axoneme extension during ciliogenesis.

Discussion

Trichoplein localizes to centrioles and suppresses the aberrant ciliogenesis by activating centriolar Aurora-A in growing cells, but disappears from the mother centrioles when cells are exposed to cell cycle signals that induce ciliogenesis by serum starvation[29]. In this study, we show that the trichoplein removal depends on UPS and that CRL3-KCTD17 targets trichoplein to proteolysis through polyubiquitylation at Lys-50 and Lys-57 during ciliogenesis. If trichoplein is stabilized at mother centrioles by treatment with proteasome inhibitors, expression of non-ubiquitylatable trichoplein mutant (K50/57R) or KCTD17 depletion, in any of these cases, ciliogenesis is blocked. Thus, the trichoplein degradation is an essential event for ciliogenesis. We also demonstrate that Aurora-A silencing completely reverse the defective ciliogenesis caused by trichoplein stabilization, indicating that the KCTD17-trichoplein-Aurora-A cascade controls ciliogenesis at the initial step of axoneme extension (summarized in Fig. 5c).

CP110 is also thought to inhibit the axonemal extension from the mother cenrioles[8,15,18,19]. Similar to trichoplein, CP110 disappears from mother centrioles during ciliogenesis and this removal is essential. However, there are numerous differences between trichoplein and CP110. In contrast to trichoplein localization at the subdistal/medial zone of centrioles[30], CP110 localizes at the distal end of centrioles and structurally caps the centriole microtubles[14]. Therefore, siRNA-mediated depletion of CP110, but not trichoplein, induces the elongation of centriolar microtubules in non-ciliated cells[12,30,45]. In addition, the CP110 loss is accompanied by a recruitment of the protein kinase

TTBK2 to the distal end of mother centrioles[19], but do not depends on proteasomal degradation (Fig. 1c), during ciliogenesis. Whether or not trichoplein-mediated and CP110-mediated regulations are mutually interrelated in axoneme extension is an interesting area for further experimentation.

CRL3-KCTD17 targets trichoplein to proteolysis in response to serum starvation, but the CRL3-KCTD17 protein levels were unchanged (Supplementary Fig. 13a). Serum starvation had less effect on the myc-KCTD17 localization (Supplementary Fig. 13b) and the trichoplein–KCTD17 interaction (Supplementary Fig. 6b). Thus, serum starvation-induced trichoplein degradation appears to require additional mechanisms. One possibility is that CRL3-KCTD17 activity may be modulated through post-translational modification like phosphorylation by MARK4 or TTBK2 (refs 18,19). Alternatively, an unidentified deubiquitylating enzyme that counteracts the trichoplein polyubiquitylation may be active in growing cells and become inactive upon serum starvation. It will be future work to investigate whether the trichoplein degradation is regulated by these protein kinases or deubiquitylating enzyme and its physiological contribution to axoneme extension during ciliogenesis.

Methods

cDNA. Human cDNAs for KCTD17 (FLJ12242), Cul3 (FLJ76583) and Rbx1 (FLJ96824) were from the Human Gene and Protein Database (HGPD). Full-length KCTD17 was amplified using PCR primers (5′-AAAAGGATCCATG CAGACGCCGCGGCCGGCGATGAGGATGGAGGCCGGGGAG-3′ and 5′-CCG GAATTCTTAGATGGGAACCCCAAGTC-3′) from FLJ12242 as a template. pCGN-HA-Ubiquitin was a kind gift from A. Kikuchi (Osaka University, Japan). Human cDNAs for trichoplein and Aurora-A were previously described[28–30]. Plasmid transfection was performed with Lipofectamine 2000 (Invitrogen) or FuGENE HD (Promega) transfection reagents in HEK293T or RPE1 cell, respectively.

Cell culture. hTERT-immortalized human retinal pigment epithelial (RPE1) cells were cultured in DMEM and F12 nutrient mix (1:1) supplemented with 10% fetal bovine serum. IMR-90 and HEK293T cells were cultured in DMEM supplemented with 10% fetal bovine serum. MG132 (0.3 μM), Lactacystin (2 μM), ALLN (10 μM) and cycloheximide (200 ng ml^{-1}) were purchased from Merck. Epoxomicin (20 nM) was obtained from Peptide Institute Inc.

Establishment of Tet-On RPE1 cell lines. Tet-On RPE1 cell lines that expressed myc-KCTD17 or MBP-trichoplein-flag (WT or K50/57R) were established with the same procedure described previously[29,46,47]. The rtTA-advanced segment and the tTS transcriptional silencer segment from pTet-On Advanced and pQC-tTS-IN (BD Clontech) were recombined into the retroviral vector pDEST-PQCXIP and pDEST-PQCXIN, respectively, by the LR reaction (Invitrogen) to generate PQCXIN-Tet-On ADV and PQCXIP-tTS. The Elongation factor 1 alpha promoter (EF) in CSII-EF-MCS (a gift from Hiroyuki Miyoshi, RIKEN BioResource Center, Tsukuba, Japan) was replaced with a Tet-responsive promoter (TRE-Tight) from pTRE-Tight (BD Clontech) followed by a modified RfA fragment (Invitrogen) to make a Tet-responsive lentivirus vector, CSII-TRE-Tight-RfA. Fusion cDNAs with siRNA-resistant KCTD17 and trichoplein were recombined into the lentiviral vector by the LR reaction (Invitrogen) to generate CSII-TRE-Tight-myc-KCTD17 and CSII-TRE-Tight-MBP-trichoplein-3xFLAG, respectively. For induction of myc-KCTD17 or MBP-trichoplein-flag, Tet-On RPE1 cells were treated with 30 or 100 ng ml^{-1} doxycycline (Sigma-Aldrich), respectively.

Protein purification. Cul3-3xFlag and Rbx1-GFP were coexpressed in HEK293T cells using Lipofectamine 2000. One day after transfection, cells were lysed in cell lysis buffer (20 mM Tris-HCl (pH 7.5), 150 mM NaCl, 2 mM β-glycerophosphate, 50 mM NaF, 1 mM Na_3VO_4, 2.5 mM sodium pyrophosphate, 2 mM EDTA, 1 mM EGTA and 1% Triton X-100) containing protease inhibitor cocktail (Nacalai Tesque). Cul3-3xFlag immunocomplexes immobilized on anti-DYKDDDDK-tag antibody beads (Wako Laboratory Chemicals) were washed three times with cell lysis buffer and twice with TBS (50 mM Tris–HCl (pH 7.4) 150 mM NaCl), and then eluted with 100 μg ml^{-1} 3xFlag peptide (Sigma-Aldrich) dissolved in PBS containing 0.1% Tween 20 (PBST). For protein purification from bacteria, GST (glutathione-S-transferase)-tagged KCTD17 and MBP-trichoplein[29] were expressed in DH5α strain (Invitrogen) and BL21 CodonPlus RP stain (Stratagene), respectively. Each protein was purified through the affinity chromatography with glutathione-sepharose 4B (GE Healthcare) or with amylose resin (NewEngland Biolabs).

Immunoprecipitation and GST pull-down assays. We performed the immunoprecipitation and GST pull-down assays using cell lysis buffer as previously described[46,47]. For immunoprecipitation, we used 5 μg of following antibody per assay: anti-GFP (GF090R)-conjugated agarose, c-Myc (MC045) agarose conjugate (Nacalai Tesque), anti-Flag (M2, Sigma-Aldrich) and anti-MBP (1G12, Medical & Biological Laboratories Co. LTD (MBL)).

***In vitro* ubiquitylation assay.** A measure of 12 μg of His-Ubiquitin (LifeSensors Inc), 1 μg of MBP-trichoplein, 0.1 μg of Cul3-3xFlag immunocomplex, 1 μg of GST-KCTD17, 0.4 μg of His-E1 (Ube1; ENZO Life Sciences) and 0.5 μg His-E2 (Ubiquitin-conjugating enzyme sampler pack; Enzo Life Sciences) were incubated in 20 μl of reaction mixture (50 mM Tris–HCl (pH7.5), 5 mM $MgCl_2$, 2 mM NaF, 2 mM ATP, 0.6 mM dithiothreitol) at 37 °C for 1 h. The reaction was subjected to immunoprecipitation using anti-trichoplein or anti-MBP before immunoblotting with anti-Ubiquitin.

***In vivo* ubiquitylation assay.** One day after transfection, cells were lysed in the denaturing condition with hot ubiquitin buffer (95 °C) containing 25 mM Tris–HCl (pH 8.0), 1.5% SDS, 0.15% sodium deoxycholate, 0.15% NP-40, 1 mM EDTA, 1 μM okadaic acid and 5 mM *N*-ethylmaleimide. The lysates were diluted (1:10) with cell lysis buffer and used for immunoprecipitation with anti-trichoplein (for endogenous trichoplein), anti-Myc (for myc-trichoplein) and anti-Flag (for MBP-trichoplein-flag). Immunoprecipitates were washed three times with cell lysis buffer containing the denaturing detergent SDS (0.1%), and then analyzed by SDS–polyacrylamide gel electrophoresis. To prevent the proteasomal degradation of polyubiquitylated trichoplein constructs, we treated cells with 10 μM MG132 in the presence or absence of serum for 6 h before cell lysis.

E3 ubiquitin ligase array. cDNA clones used to screen for E3 ubiquitin ligase to trichoplein were selected from the HuPEX library[39,48]. We selected 744 genes to be human E3 ubiquitin ligase by a keyword search of the HGPD (http://www.HGPD.jp/)[38], Swiss-Prot database and few papers[49–51]. We have 622 genes to these 744 genes, which were corresponding to 1,172 HuPEX clones containing variant clones (Supplementary Table 1). These HuPEX clones were transferred to the pEW-FG expression vector[39] harbouring FLAG and GST tags by using the Gateway LR reaction. The protein synthesis was performed by the method of wheat germ protein expression system according to the manufacturer instructions[39] (CellFree Sciences). Protein array system by using magnetic beads is indicated in Supplementary Fig. 4a. The magnetic beads with glutathione ligand (Promega) were added to reaction mixture containing synthesized protein having FLAG-GST tag, and the synthesized protein was absorbed on the surface of magnetic beads. Beads adsorbed synthesized protein dispensed on the magnet plate (MEIHO Co. Ltd.), which have magnet at the bottom of each well. Each E3 ubiquitin ligase was immobilized at the bottom of magnetic plate via magnetic beads in solution. By using this E3 ubiquitin ligase array, we screened the specific E3 ubiquitin ligase for trichoplein. The array was blocked with PBST and 1% BSA (PBST + BSA). The array was incubated for 1 h at 25 °C with MBP-trichoplein (1.0 mg ml^{-1} in PBST + BSA), then washed in PBST. The array was incubated with HRP-conjugated anti-MBP tag sheep antibody (GE Healthcare; diluted 1:1,000 in PBST + BSA), washed in PBST. Reactive spots were detected with ECL plus (GE Healthcare). The quantity of protein on each spot was assayed by using FLAG M2-Peroxidase (*HRP*)-conjugated monoclonal antibody (Sigma-Aldrich). Reactive spots were normalized by each quantity of protein on each spot.

Immunoblotting. We performed the immunoblotting as described[46,47]. For immunoblotting, we produced a rabbit polyclonal anti-KCTD17 antibody by immunizing bacterially purified KCTD17 (193–297aa) protein (MBL) and a rabbit polyclonal antibody for trichoplein[29]. The list of antibodies with source and conditions of immunoblotting is shown in Supplementary Table 2. In some immunoblotting experiments, we used Can Get Signal immunoreaction enhancer solutions (TOYOBO) for dilution of primary and secondary antibodies. Band intensities were analyzed by densitometry (ImageJ 1.43r, for Macintosh OS X; National Institute of Health, Bethesda, MD, USA). Uncropped versions of the most important blots are shown in Supplementary Figs 14 and 15.

Microscopy. Immunofluoresence microscopy was performed using confocal microscopy (LSM510 META; Carl Zeiss) equipped with a microscope (Axiovert 200 M; Carl Zeiss), a plan Apochromat × 100/1.4 NA oil immersion lens and LSM image Browser software (Carl Zeiss) as described[29] with slight modifications. The list of antibodies with source and conditions of indirect immunofluorescence is shown in Supplementary Table 2. In some immunofluorescence experiments, we used Can Get Signal immunostain Solution A (TOYOBO). For induction of primary cilia, RPE1 and IMR-90 cells were seeded on sterile coverslips, grown for 1 day and then subjected to serum starvation. For detection of primary cilia, cells were placed on ice for 20–30 min before fixation with cold methanol, and stained with anti-acetylated tubulin antibody[29]. BrdU incorporation was evaluated using DNA Replication Assay Kit (Millipore). Quantification of fluorescence intensity was performed using ImageJ 1.45r software.

Transmission electron microscopy. RPE1 cells cultured on coverslips were fixed with 2% fresh formaldehyde and 2.5% glutaraldehyde in 0.1 M sodium cacodylate buffer (pH 7.4) for 2 h at room temperature. After washing with 0.1 M cacodylate buffer (pH 7.4), they were postfixed with ice-cold 1% OsO_4 in the same buffer for 2 h. The samples were rinsed with distilled water, stained with 0.5% aqueous uranyl acetate for 2 h or overnight at room temperature, dehydrated with ethanol and propylene oxide, and embedded in an embedding kit (Poly/Bed 812; PolySciences, Inc.). After removal of coverslips using ice-cold hydrofluoric acid, ultra-thin sections were cut, doubly stained with uranyl acetate and Reynolds's lead citrate, and viewed with a transmission electron microscope (JEM-1010; JEOL) with a charge-coupled device camera (BioScan model 792; Gatan, Inc.) at an accelerating voltage of 100 kV.

SiRNAs. Transfection of siRNA duplexes (final concentration, 20 nM) was performed with Lipofectamine RNAiMAX reagent according to the reverse transfection protocol (Invitrogen). All siRNA duplexes were purchased from Qiagen. Target sequences are listed in Supplementary Table 3.

References

1. Nigg, E. A. & Raff, J. W. Centrioles, centrosomes, and cilia in health and disease. *Cell* **139,** 663–678 (2009).
2. Goetz, S. C. & Anderson, K. V. The primary cilium: a signalling centre during vertebrate development. *Nat. Rev. Genet.* **11,** 331–344 (2010).
3. Ishikawa, H. & Marshall, W. F. Ciliogenesis: building the cell's antenna. *Nat. Rev. Mol. Cell Biol.* **12,** 222–234 (2011).
4. Sorokin, S. Centrioles and the formation of rudimentary cilia by fibroblasts and smooth muscle cells. *J. Cell Biol.* **15,** 363–377 (1962).
5. Molla-Herman, A. *et al.* The ciliary pocket: an endocytic membrane domain at the base of primary and motile cilia. *J. Cell Sci.* **123,** 1785–1795 (2010).
6. Sorokin, S. P. Reconstructions of centriole formation and ciliogenesis in mammalian lungs. *J. Cell. Sci.* **3,** 207–230 (1968).
7. Nigg, E. A. & Stearns, T. The centrosome cycle: centriole biogenesis, duplication and inherent asymmetries. *Nat. Cell Biol.* **13,** 1154–1160 (2011).
8. Kobayashi, T. & Dynlacht, B. D. Regulating the transition from centriole to basal body. *J. Cell Biol.* **193,** 435–444 (2011).
9. Goto, H., Inoko, A. & Inagaki, M. Cell cycle progression by the repression of primary cilia formation in proliferating cells. *Cell. Mol. Life Sci.* **70,** 3893–3905 (2013).
10. Plotnikova, O. V., Golemis, E. A. & Pugacheva, E. N. Cell cycle-dependent ciliogenesis and cancer. *Cancer Res.* **68,** 2058–2061 (2008).
11. Mikule, K. *et al.* Loss of centrosome integrity induces p38-p53-p21-dependent G1-S arrest. *Nat. Cell Biol.* **9,** 160–170 (2007).
12. Schmidt, T. I. *et al.* Control of centriole length by CPAP and CP110. *Curr. Biol.* **19,** 1005–1011 (2009).
13. Tsang, W. Y. *et al.* CP110 suppresses primary cilia formation through its interaction with CEP290, a protein deficient in human ciliary disease. *Dev. Cell* **15,** 187–197 (2008).
14. Kleylein-Sohn, J. *et al.* Plk4-induced centriole biogenesis in human cells. *Dev. Cell* **13,** 190–202 (2007).
15. Spektor, A., Tsang, W. Y., Khoo, D. & Dynlacht, B. D. Cep97 and CP110 suppress a cilia assembly program. *Cell* **130,** 678–690 (2007).
16. Kim, J. *et al.* Functional genomic screen for modulators of ciliogenesis and cilium length. *Nature* **464,** 1048–1051 (2010).
17. Majumder, S. & Fisk, H. A. VDAC3 and Mps1 negatively regulate ciliogenesis. *Cell Cycle* **12,** 849–858 (2013).
18. Kuhns, S. *et al.* The microtubule affinity regulating kinase MARK4 promotes axoneme extension during early ciliogenesis. *J. Cell Biol* **200,** 505–522 (2013).
19. Goetz, S. C., Liem, K. F. Jr. & Anderson, K. V. The spinocerebellar ataxia-associated gene tau tubulin kinase 2 controls the initiation of ciliogenesis. *Cell* **151,** 847–858 (2012).
20. Tang, Z. *et al.* Autophagy promotes primary ciliogenesis by removing OFD1 from centriolar satellites. *Nature* **502,** 254–257 (2013).
21. Hershko, A. & Ciechanover, A. The ubiquitin system. *Annu. Rev. Biochem.* **67,** 425–4795 (1998).
22. Ciechanover, A., Orian, A. & Schwartz, A. L. Ubiquitin-mediated proteolysis: biological regulation via destruction. *Bioessays* **22,** 442–451 (2000).
23. Thoma, C. R. *et al.* pVHL and GSK3β are components of a primary cilium-maintenance signalling network. *Nat. Cell Biol.* **9,** 588–595 (2007).
24. Xu, J. *et al.* VHL inactivation induces HEF1 and Aurora kinase A. *J. Am. Soc. Nephrol.* **21,** 2041–2046 (2010).
25. Villumsen, B. H. *et al.* A new cellular stress response that triggers centriolar satellite reorganization and ciliogenesis. *EMBO J.* **32,** 3029–3040 (2013).
26. Patil, M., Pabla, N., Huang, S. & Dong, Z. Nek1 phosphorylates Von Hippel-Lindau tumor suppressor to promote its proteasomal degradation and ciliary destabilization. *Cell Cycle* **12,** 166–1713 (2013).
27. Huang, K., Diener, D. R. & Rosenbaum, J. L. The ubiquitin conjugation system is involved in the disassembly of cilia and flagella. *J. Cell Biol.* **186,** 601–613 (2009).
28. Nishizawa, M. *et al.* Identification of trichoplein, a novel keratin filament-binding protein. *J. Cell Sci.* **118,** 1081–1090 (2005).
29. Inoko, A. *et al.* Trichoplein and Aurora A block aberrant primary cilia assembly in proliferating cells. *J. Cell Biol.* **197,** 391–405 (2012).
30. Ibi, M. *et al.* Trichoplein controls microtubule anchoring at the centrosome by binding to Odf2 and ninein. *J. Cell Sci.* **124,** 857–864 (2011).
31. Vecchione, A. *et al.* MITOSTATIN, a putative tumor suppressor on chromosome 12q24.1, is downregulated in human bladder and breast cancer. *Oncogene* **28,** 257–269 (2008).
32. Cerqua, C. *et al.* Trichoplein/mitostatin regulates endoplasmic reticulum–mitochondria juxtaposition. *EMBO Rep.* **11,** 854–860 (2010).
33. Pugacheva, E. N., Jablonski, S. A., Hartman, T. R., Henske, E. P. & Golemis, E. A. HEF1-dependent Aurora A activation induces disassembly of the primary cilium. *Cell* **129,** 1351–1363 (2007).
34. Nakagawa, Y., Yamane, Y., Okanoue, T. & Tsukita, S. Outer dense fiber 2 is a widespread centrosome scaffold component preferentially associated with mother centrioles: its identification from isolated centrosomes. *Mol. Biol. Cell* **12,** 1687–1697 (2001).
35. Thomas, J. *et al.* Transcriptional control of genes involved in ciliogenesis: a first step in making cilia. *Biol. Cell* **102,** 499–513 (2010).
36. Bonnafe, E. *et al.* The transcription factor RFX3 directs nodal cilium development and left-right asymmetry specification. *Mol. Cell Biol.* **24,** 4417–4427 (2004).
37. Benos, P. V., Hoh, R. A., Stowe, T. R., Turk, E. & Stearns, T. Transcriptional program of ciliated epithelial cells reveals new cilium and centrosome components and links to human disease. *PLoS ONE* **7,** e52166 (2012).
38. Maruyama, Y. *et al.* Human Gene and Protein Database (HGPD): a novel database presenting a large quantity of experiment-based results in human proteomics. *Nucleic Acids Res.* **37,** D762–D766 (2009).
39. Goshima, N. *et al.* Human protein factory for converting the transcriptome into an in vitro-expressed proteome. *Nat. Methods* **5,** 1011–1017 (2008).
40. Genschik, P., Sumara, I. & Lechner, E. The emerging family of CULLIN3-RING ubiquitin ligases (CRL3s): cellular functions and disease implications. *EMBO J.* **32,** 2307–2320 (2013).
41. Furukawa, M., He, Y. J., Borchers, C. & Xiong, Y. Targeting of protein ubiquitination by BTB-Cullin 3-Roc1 ubiquitin ligases. *Nat. Cell Biol.* **5,** 1001–1007 (2003).
42. Pintard, L. *et al.* The BTB protein MEL-26 is a substrate-specific adaptor of the CUL-3 ubiquitin-ligase. *Nature* **425,** 311–316 (2003).
43. Xu, L. *et al.* BTB proteins are substrate-specific adaptors in an SCF-like modular ubiquitin ligase containing CUL-3. *Nature* **425,** 316–321 (2003).
44. Ye, Y. & Rape, M. Building ubiquitin chains: E2 enzymes at work. *Nat. Rev. Mol. Cell Biol.* **10,** 755–764 (2009).
45. Kohlmaier, G. *et al.* Overly long centrioles and defective cell division upon excess of the SAS-4-related protein CPAP. *Curr. Biol.* **19,** 1012–1018 (2009).
46. Kasahara, K. *et al.* 14-3-3gamma mediates Cdc25A proteolysis to block premature mitotic entry after DNA damage. *EMBO J.* **29,** 2802–2812 (2010).
47. Kasahara, K. *et al.* PI 3-kinase-dependent phosphorylation of Plk1-Ser99 promotes association with 14-3-3gamma and is required for metaphase-anaphase transition. *Nat. Commun.* **4,** 1882 (2013).
48. Maruyama, Y. *et al.* HGPD: Human Gene and Protein Database, 2012 update. *Nucleic Acids Res.* **40,** D924–D929 (2012).
49. Li, W. *et al.* Genome-wide and functional annotation of human E3 ubiquitin ligases identifies MULAN, a mitochondrial E3 that regulates the organelle's dynamics and signaling. *PLoS One* **3,** e1487 (2008).
50. Bosu, D. R. & Kipreos, E. T. Cullin-RING ubiquitin ligases: global regulation and activation cycles. *Cell Div.* **3,** 7 (2008).
51. Peters, J. M. The anaphase promoting complex/cyclosome: a machine designed to destroy. *Nat. Rev. Mol. Cell Biol.* **7,** 644–656 (2006).

Acknowledgements

We thank K. Kikuchi (Osaka University, Japan) for providing pCGN-HA-Ubiquitin. We are indebted to Y. Tomono (Shigei Medical Research Institute) for the antibody production. We are also grateful to H. Goto and M. Ibi for purification of MBP-trichoplein; I. Izawa, A. Inoko, M. Matsuyama and H. Inaba for technical comments; E. Kawamoto, Y. Hayashi, K. Kobori and C. Yuhara for technical assistance; Y. Takada for secretarial expertise; and B. Omary (University of Michigan Medical School, USA) for critical comments on the manuscript. This work was supported in part by Grants-in-Aid for Scientific Research from the Japan Society for the Promotion of Science and from the Ministry of Education, Science, Technology, Sports and Culture of Japan; and the Takeda Science Foundation.

Author contributions

M.I. conceived the project. K.K. and M.I. interpreted data and wrote the manuscript. K.K. performed much of the experiments. K.K., T.K, S.E. and F.M. provided experimental

materials. Y.-t.K., Y.-f.K. and N.G. conducted protein array screen. S.Y. executed TEM analysis.

Additional information

Supplementary Information accompanies this paper at http://www.nature.com/naturecommunications

Competing financial interests: The authors declare no competing financial interests.

Reprints and permission information is available online at http://npg.nature.com/reprintsandpermissions/

How to cite this article: Kasahara, K. *et al.* Ubiquitin-proteasome system controls ciliogenesis at the initial step of axoneme extension. *Nat. Commun.* 5:5081 doi: 10.1038/ncomms6081 (2014).

SCIENTIFIC REPORTS

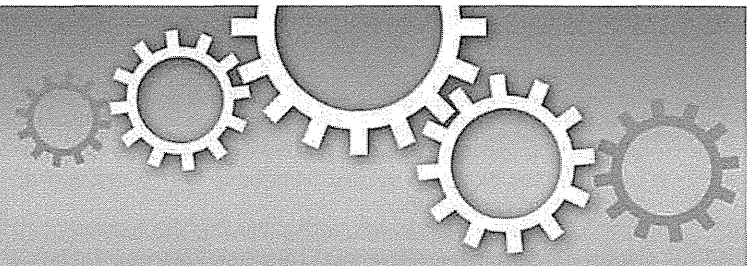

OPEN

SUBJECT AREAS:
PLURIPOTENT STEM CELLS
INDUCED PLURIPOTENT STEM CELLS

Received
18 July 2014

Accepted
14 November 2014

Published
4 December 2014

Correspondence and requests for materials should be addressed to K.-I.T. (tezuka@gifu-u.ac.jp)

The homeobox gene *DLX4* promotes generation of human induced pluripotent stem cells

Naritaka Tamaoki[1], Kazutoshi Takahashi[2], Hitomi Aoki[3], Kazuki Iida[1], Tomoko Kawaguchi[1], Daijirou Hatakeyama[1], Masatoshi Inden[4], Naoyuki Chosa[5], Akira Ishisaki[5], Takahiro Kunisada[3], Toshiyuki Shibata[1], Naoki Goshima[6], Shinya Yamanaka[2] & Ken-ichi Tezuka[3]

[1]Department of Oral and Maxillofacial Science, Gifu University Graduate School of Medicine, 1-1 Yanagido, Gifu City, Gifu 501-1194, Japan, [2]Center for iPS Cell Research and Application, Kyoto University, 53 Kawahara-cho, Shogoin, Sakyo-ku, Kyoto 606-8507, Japan, [3]Department of Tissue and Organ Development, Gifu University Graduate School of Medicine, 1-1 Yanagido, Gifu City, Gifu 501-1194, Japan, [4]Laboratory of Medical Therapeutics and Molecular Therapeutics, Gifu Pharmaceutical University, 1-25-4 Daigaku-Nishi, Gifu 501-1195, Japan, [5]Division of Cellular Biosignal Sciences, Department of Biochemistry, Iwate Medical University, 19-1 Uchimaru, Morioka, Iwate 020-8505, Japan, [6]Molecular Profiling Research Center for Drug Discovery, National Institute of Advanced Industrial Science and Technology, 2-4-7 Aomi, Koto-ku, Tokyo 135-0064, Japan.

The reprogramming of somatic cells into induced pluripotent stem cells (iPSCs) by defined transcription factors has been a well-established technique and will provide an invaluable resource for regenerative medicine. However, the low reprogramming efficiency of human iPSC is still a limitation for clinical application. Here we showed that the reprogramming potential of human dental pulp cells (DPCs) obtained from immature teeth is much higher than those of mature teeth DPCs. Furthermore, immature teeth DPCs can be reprogrammed by OCT3/4 and SOX2, conversely these two factors are insufficient to convert mature teeth DPCs to pluripotent states. Using a gene expression profiles between these two DPC groups, we identified a new transcript factor, distal-less homeobox 4 (DLX4), which was highly expressed in immature teeth DPCs and significantly promoted human iPSC generation in combination with OCT3/4, SOX2, and KLF4. We further show that activation of TGF-β signaling suppresses the expression of DLX4 in DPCs and impairs the iPSC generation of DPCs. Our findings indicate that DLX4 can functionally replace c-MYC and supports efficient reprogramming of immature teeth DPCs.

Previous reports showed that induced pluripotent stem cells (iPSCs) can be generated from various types of somatic cells using a combination of transcription factors, such as OCT3/4, SOX2, KLF4, c-MYC, NANOG, and LIN28[1–14]. Although these reports indicated that iPSCs can be induced from many types of somatic cells, the backgrounds of the donor cells, such as gene expression patterns and the epigenetic state, have a significant impact on the reprogramming efficiency, kinetics, and the transcription factors required for the induction[3,5,7,13–16]. Because reprogramming of differentiated cells involves gradual changes in gene expression patterns, cell morphology, and epigenetic state towards the embryonic state[17–21], it has been assumed that stem cells and progenitor cells are more amenable to reprogramming than that of more differentiated cells[5,12,16,22,23]. For example, mouse and human neural stem cells can be reprogrammed with the single transcription factor OCT3/4[16,24]. Similarly, Eminli et al. reported that hematopoietic stem and progenitor cells gave rise to iPSCs up to 300 times more efficiently than terminally differentiated B and T cells did, suggesting that the differentiation state of the starting cells affects reprogramming efficiency[23]. However, these stem/progenitor cells are generally inaccessible, require complicated procedures to obtain, and are difficult to propagate *in vitro*.

Human dental pulp cells (DPCs) are obtained easily from adult teeth discarded as medical waste and contain abundant stem like cells[25–29]. In addition, DPCs can be expanded in a simple culture condition and show continuous growth for up to 30 passages[28]. In a previous study, we established more than 150 DPC lines isolated from extracted wisdom teeth and evaluated the potential of DPCs for iPS cell banking[14,28]. The donor teeth of these DPC lines were categorized into three developmental stages: crown completed (CC), root forming (RF), and root completed (RC). We randomly selected six lines isolated from various developmental stages to induce iPSCs and found that five DPC lines showed higher reprogramming efficiency than human dermal fibroblasts (HDFs). In

this study, it remained unclear why DP75, isolated from the oldest patient in the RC stage, showed remarkably low reprogramming efficiency similar to HDFs.

Here, we focused on the relationship between the developmental stages of DPCs and reprogramming efficiency. We found that DPCs in the mature (RC) stage were reprogrammed less efficiently than DPCs in the immature (CC and RF) stages.

Results

DPCs isolated from immature teeth can be reprogrammed into iPSCs using two factors. First, we attempted to generate iPSCs from DP31 cells, a cell line isolated from the immature (CC) stage of teeth, using as few transcription factors as possible. We found that only two factors, OCT3/4 and SOX2 (OS), are required to induce ES-cell-like colonies repeatedly, albeit with very low frequency compared to the combination of OCT3/4, SOX2, and KLF4 (OSK) (Fig. 1a). Similarly, we obtained iPSCs from other immature tooth DPCs, such as DP1 (CC stage) and DP87 (RF stage), with only two factors (data not shown). Genomic PCR was employed to demonstrate that OS-induced iPSCs derived from DP31 cells (iPS-DP31-OS) contained only OCT3/4 and SOX2 transgenes (Fig. 1b). We also confirmed that iPS-DP31-OS cells could be expanded easily and expressed human specific pluripotency markers (Fig. 1c). These cells differentiated into

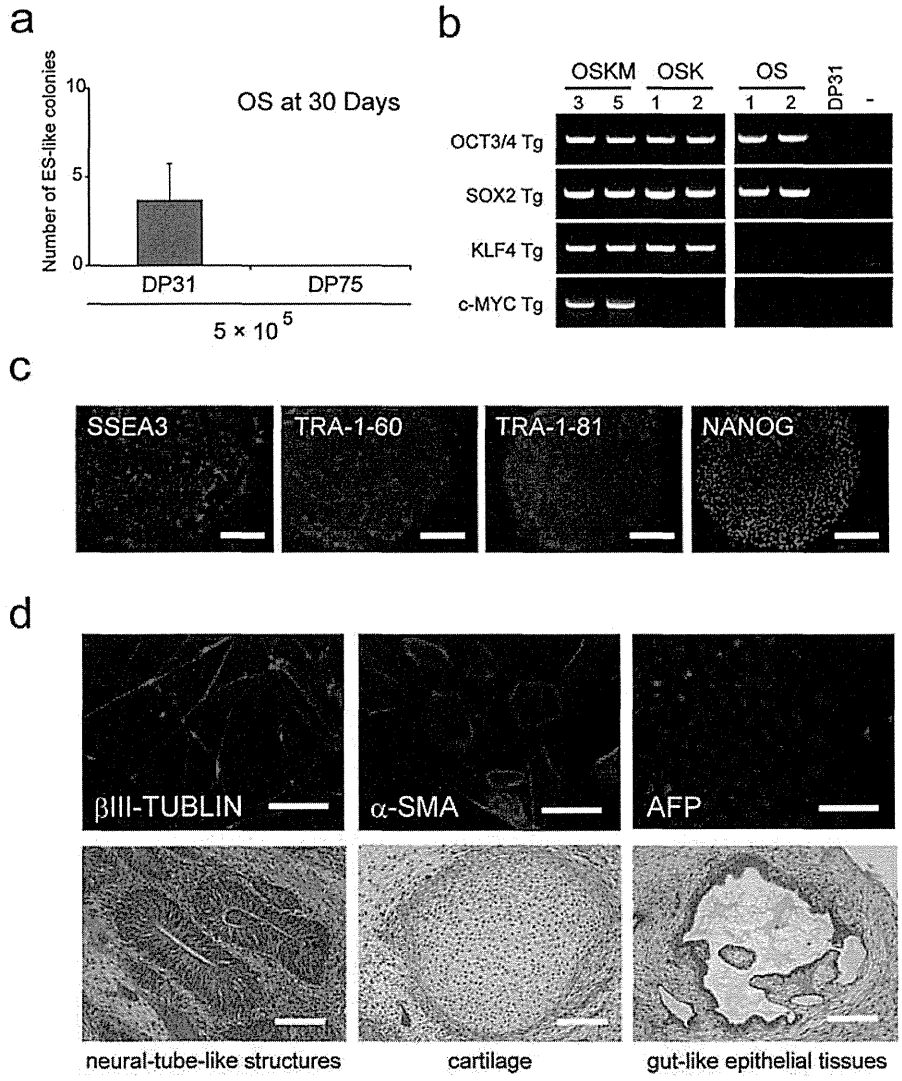

Figure 1 | DP31 cells can be reprogrammed to iPSCs using OCT3/4 and SOX2. (a) We obtained a few ES-cell-like colonies from 5×10^5 DP31 cells transduced with OCT3/4 and SOX2 (OS), but we could not obtain any ES-cell-like colonies from DP75 cells. Human ES-cell-like colonies were counted at 30 days post infection. Error bars indicate ± S.D. (n = 3). (b) Genomic PCR using transgene-specific primers, with DP31 cells as a negative control, confirmed the insertion of only two transgenes in iPSCs derived from DP31 cells transduced with OS (iPS-DP31-OS) by PCR. The numbers denote different iPSC lines. We cropped the gels and blots for clarifying our presentation. The gels have been run under the same experimental conditions. (c) iPS-DP31-OS cells expressed pluripotency markers including SSEA3, TRA-1-60, TRA-1-81, and NANOG. Scale bar = 100 μm. (d) Pluripotency of iPS-DP31-OS cells was confirmed by EB-mediated differentiation and teratoma formation assay. Immunofluorescence staining showed that EB structures derived from iPS-DP31-OS cells expressed markers characteristic of the three germ layers including βIII-tubulin (ectoderm), α-smooth-muscle actin (mesoderm), and α-fetoprotein (endoderm). Nuclei were stained with Hoechst 33342. Scale bar = 100 μm. Hematoxylin- and eosin-stained sections of teratomas generated from iPS-DP31-OS cells are shown in the lower panels. The teratomas contained various tissues of all three germ layers, such as neural-tube-like structures (ectoderm), cartilage (mesoderm), and gut-like epithelial tissue (endoderm). Abbreviations: AFP, alpha-fetoprotein; α-SMA, alpha smooth muscle actin. Scale bar = 100 μm.

all the three germ layers *in vitro* and *in vivo* (Fig. 1d). However, we did not obtain any ES-cell-like colonies from DP75, a line obtained from the mature (RC) stage of the tooth, using the OS cocktail (Fig. 1a). These results compelled us to further examine the maturation stage dependency of DPC reprogramming.

Statistical comparison of reprogramming potency between immature and mature tooth DPCs. To confirm that the reprogramming potency of DPC lines was dependent on the developmental stage but not on simple individual differences of donor teeth, we selected an additional five DPC lines (nine lines in total) isolated from various developmental stages (Supplementary Fig. S1) and introduced Yamanaka's four factors (OCT3/4, SOX2, KLF4, c-MYC; OSKM) into them using a retroviral gene-delivery system. Human ES-cell-like colonies were morphologically identified and counted at 21 days post-infection as previously described[1,14]. The number of human ES-cell-like colonies obtained from each DPC line was normalized to that of DP31 cells. All DPC lines isolated from the immature teeth (CC and RF stages) group showed significantly higher reprogramming efficiency than the lines isolated from mature (RC stage) teeth (Fig. 2a).

Identification of differentially expressed genes in DPCs isolated from immature and mature teeth. The results of the reprogramming experiments prompted us to compare the gene expression profiles of DPCs from mature and immature teeth. To avoid masking of target genes by sex-related genes, we chose eight DPC lines isolated from male donors (four lines from individuals with immature teeth and four lines from individuals with mature teeth) (Supplementary Fig. S1). Among the 28 genes significantly up-regulated by more than five-fold in immature teeth DPCs (Supplementary Table S1), we focused on the homeobox gene *Dlx4*, the expression of which was up-regulated 35-fold in immature teeth DPCs on average and was thus the most differentially expressed transcription factor.

We performed a real-time PCR assay to evaluate the transcript levels of DLX4 in each DPC line. As expected, the transcript levels of DLX4 in DPCs from immature teeth were much higher than those of mature teeth DPCs and HDFs (Fig. 2b). Moreover, the transcript levels of DLX4 in all immature teeth DPCs were similar to those of human ES cells (hKES).

Ectopic expression of *DLX4* promotes human iPSC generation. We next studied whether ectopic expression of DLX4 could increase

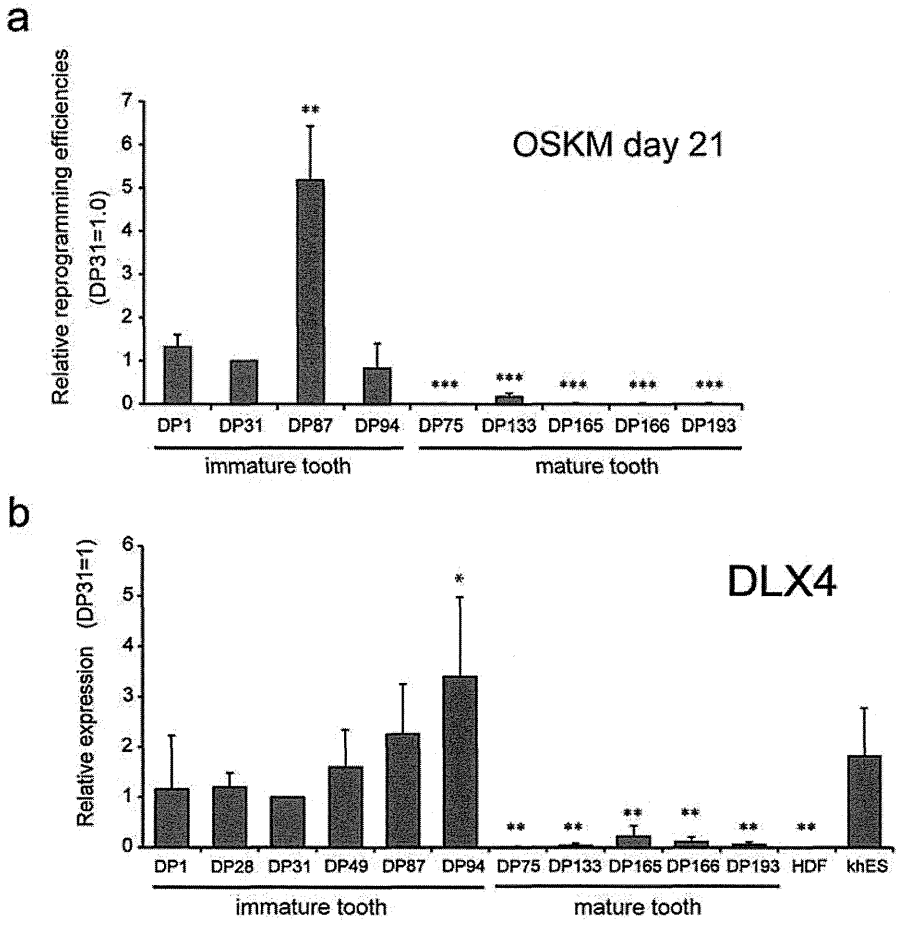

Figure 2 | DPCs from immature teeth were more amenable to reprogramming than DPCs from mature teeth and showed high expression levels of endogenous DLX4. (a) Nine DPC lines were selected for evaluation of reprogramming potency. The four Yamanaka factors (OSKM) were introduced by a retroviral system, and the induced human ES-cell-like colonies were counted at 21 days post infection. The number of human ES-cell-like colonies obtained from each DPC line was normalized against that obtained from DP31 cells. Error bars indicate ± S.D. (n = 3). Asterisks indicate statistical significance: *P < 0.05, ** P < 0.01, and *** P < 0.001 compared to DP31 values. (b) The transcript levels of endogenous DLX4 were quantified using real-time RT-PCR. DPCs from immature teeth showed significantly higher levels of endogenous DLX4 than DPCs from mature teeth. Moreover, the transcript levels of DLX4 in all immature teeth DPCs were similar to those of human ES cells (hKES). GAPDH was used as an internal control. Error bars indicate ± S.D. (n = 3). Asterisks indicate statistical significance: *P < 0.05, ** P < 0.01, and *** P < 0.001 compared to values from DP31 cells.

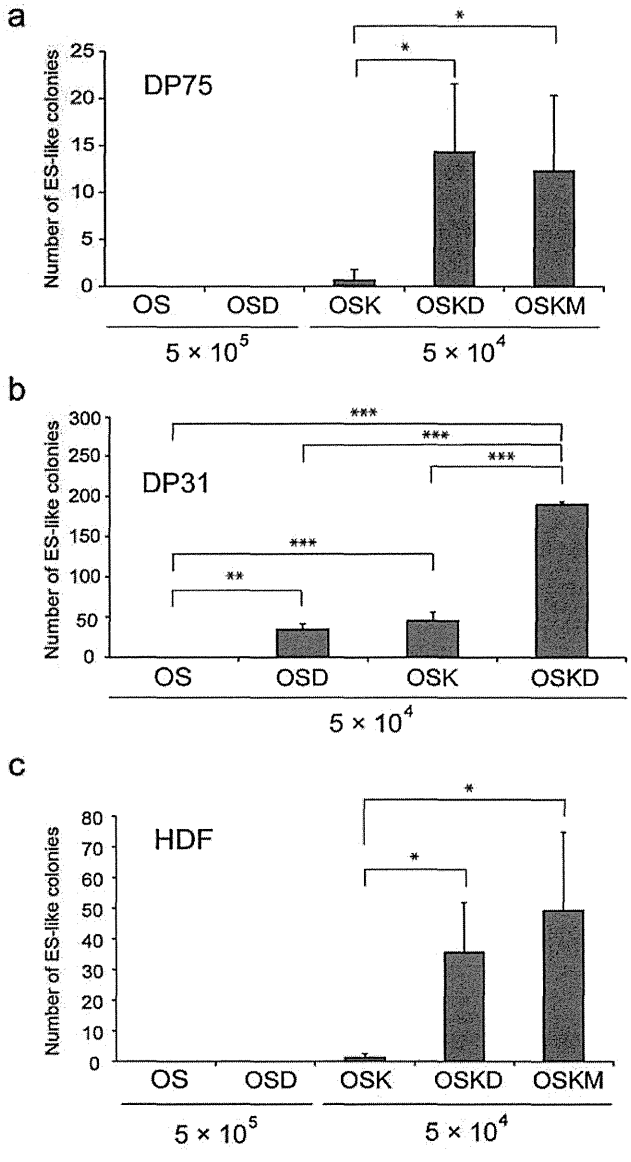

Figure 3 | Ectopic expression of DLX4 promoted human iPSC generation. (a-c) Numbers of human ES-cell-like colonies obtained from DPCs and HDFs. Human ES-cell-like colonies isolated from 5×10^5 or 5×10^4 infected cells were counted at 30 days post infection. Error bars indicate ± S.D. (n = 3). Asterisks indicate statistical significance; *P < 0.05, **P < 0.01, and ***P < 0.001.

the reprogramming efficiency of DPCs. Because we could not obtain any ES-cell-like colonies from mature teeth DPCs using the OS combination, we tried co-expression of DLX4 with OS (OSD) to convert DP75 into pluripotent cells. Contrary to our expectation, we could not obtain any ES-cell-like colonies from DP75 using the OSD cocktail (Fig. 3a). However, we observed a synergistic increase in the number of ES-cell-like colonies when both DLX4 and KLF4 were co-introduced with OS (OSKD) (~0.03%). The number of ES-cell-like colonies obtained from DP75 with OSKD was similar to the number obtained using OSKM (Fig. 3a). Next, we addressed whether ectopic expression of DLX4 could produce a similar effect during the reprogramming of DP31 cells obtained from immature teeth. As observed in DP75 cells, ectopic expression of DLX4 enhanced the reprogramming efficiency of DP31 cells (Fig. 3b). Although we could not obtain any ES-like colonies from 5×10^4 introduced DP31 cells with OS combination, we could obtain about 30 ES-like colonies constantly by using OSD combination. The OSD combination increased the reprogramming efficiency of DP31 (~0.07%) to the same level provided by OSK (Fig. 3b). As observed in DPCs, the OSKD cocktail increased the reprogramming efficiency in HDF cells to the same level observed using OSKM, although we did not obtain any ES-cell-like colonies with OSD alone, as observed for DP75 cells (Fig. 3c). Our results indicate that ectopic expression of DLX4 enhances reprogramming efficiency in combination with OCT3/4 and SOX2, similarly to KLF4. Notably, we found that use of the OSKD combination not only enhanced reprogramming, but also prevented the generation of non-ES-cell-like colonies to a greater extent than was observed with OSKM (Supplementary Fig. S2).

To determine whether enhanced reprogramming efficiency by DLX4 overexpression could result in stable establishment of iPSC lines, we picked nine ES-cell-like colonies derived from DP31 with OSD (termed iPS-DP31-OSD) for further examination. Among them, eight colonies were successfully expanded. Immunostaining confirmed the expression of pluripotent markers, including OCT3/4, SSEA4, TRA-1-60, and TRA-1-81, at levels similar to those in human ES cells (Supplementary Fig. S3a). Using real-time PCR analysis, we found that transcript levels of the pluripotency markers OCT3/4 (endogenous), NANOG, and REX1 were markedly increased in iPS-DP31-OSD lines relative to the parental cells and were similar to the transcript levels in human ES cells (Supplementary Fig. S3b). Differentiation potential towards the three germ layers was also confirmed *in vitro* and *in vivo* (Supplementary Fig. S3c).

Activation of TGF-β signal suppresses the expression level of DLX4 in DPCs and impairs iPSC generation from DPCs. Previous reports showed that MET (mesenchymal-to-epithelial transition) is a crucial early process for direct reprogramming of mouse fibroblasts to pluripotent status and that ectopic expression of KLF4 potently induced CDH1 (E-cadherin) mRNA to promote MET[19,20,30]. Similarly, KLF4 alone robustly induced CDH1 in DP31 cells as previously reported with mouse fibroblasts[20,30] (Supplementary Fig. S4a). Interestingly, ectopic expression of DLX4 also up-regulated CDH1. However, the potency of CDH1 mRNA up-regulation appeared to be lower than that of KLF4. Recent reports showed that using an inhibitor of TGF-β signaling, which promotes EMT (epithelial to mesenchymal transition), could enhance iPSC generation from mouse and human fibroblasts[20,31–33]. We then attempted to address whether TGF-β signaling could affect nuclear reprogramming of DPCs. Interestingly, the expression level of endogenous DLX4 in DPCs was suppressed by TGF-β signaling (Fig. 4a). Moreover, addition of TGF-β1 dramatically reduced the number of iPSC colonies obtained from DP1 and DP31 cells (Fig. 4b). Our results indicated that activation of TGF-β signaling suppresses the expression of DLX4 in DPCs and impairs the generation of iPSC from DPCs.

Since TGF-β signal also plays a crucial role in regulation of the cell cycle[34,35] and acceleration of cell cycle is a crucial process in early stage of reprogramming[21]. Next, we addressed whether enforced expression of DLX4 could affect the cell cycle in DPCs. Firstly, we tested whether enforced expression of DLX4 can activate endogenous expression of c-MYC in DPCs, because of its potential to replace c-MYC during nuclear reprogramming. Contrary to our expectations, we could not observe the up-regulation of c-MYC in DLX4 induced DP31 cells (Supplementary Fig. S4b). Similar to this, we also could not observe the down-regulation of CDK inhibitors by ectopic expression of DLX4, even with the combination of OSK (Supplementary Fig. S4b). Our results indicated that DLX4 does not accelerate cell growth in the early stage of reprogramming to promote iPSC generation.

Discussion

In this study, we have identified a new transcription factor, DLX4, also known as DLX7 or BP1, which promotes human iPSC generation in

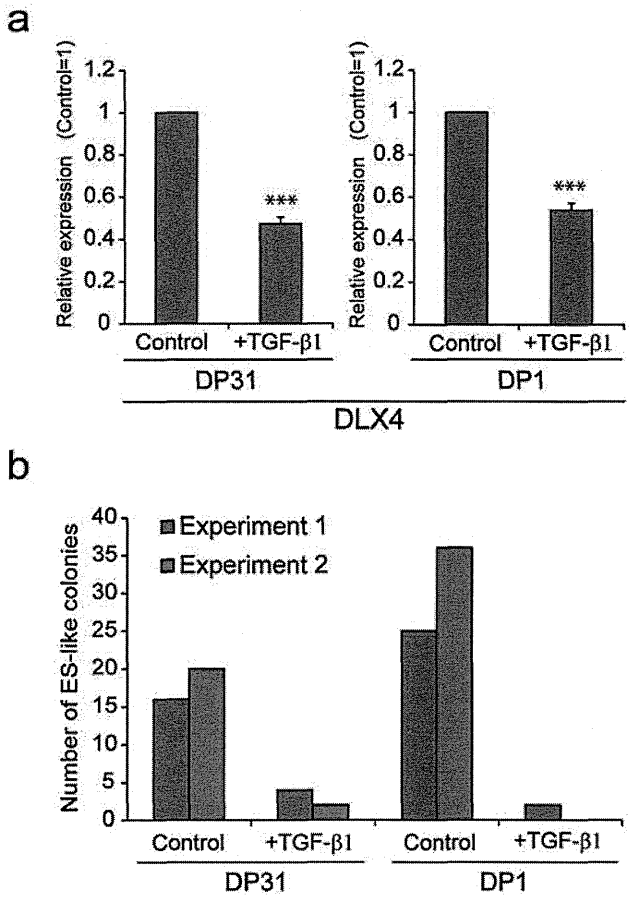

Figure 4 | Activation of TGF-β signal suppressed the expression level of DLX4 in DPCs and impaired the generation of iPSCs from DPCs. (a) DP1 and DP31 cells were cultured in DPC culture medium with TGF-β1 (5 ng/mL) or with acetic acid (as a control) for 48 h. Real-time PCR analysis showed that after activation of TGF-β signal, the transcript levels of DLX4 were down-regulated in both DP1 and DP31 cells. GAPDH was used as an internal control. Error bars indicate ± S.D. (n = 3). Asterisks indicate statistical significance; ***P < 0.001 (b) Human ES-cell-like colonies isolated from 5×10^4 infected cells (OSKM) were counted at 21 days post infection. Numbers of human ES-cell-like colonies obtained from DP1 and DP31 were dramatically reduced when TGF-β1 (5 ng/mL) was added during the reprogramming process.

combination with the classical Yamanaka factors. In mammals, the *Dlx* gene family consists of six members that are organized into three closely linked pairs: *Dlx1*/*Dlx2*, *Dlx5*/*Dlx6*, and *Dlx3*/*Dlx4*[36–38]. These *Dlx* genes play crucial roles in early development[39–42] and are known to be expressed in cranial neural crest cells and later in the craniofacial mesenchyme[43]. In this study, we found that DPCs isolated from developing teeth in the CC or RF stage show high expression of DLX4. Some reports have demonstrated that *Dlx* genes are associated with mammalian tooth formation[39,44], and indicated that DLX4 is closely related to abnormal human tooth formation. For example, a mutation of DLX3, which is the partner of DLX4, is associated with tricho-dento-osseous (TDO) syndrome and disrupts odontoblast polarization and dentin formation[45]. Therefore, it is conceivable that DLX4 is highly expressed in DPCs isolated from third molar teeth, which are still under development even after birth.

Previously, Maekawa et al. attempted to identify new transcription factors with the ability to replace Klf4 during nuclear reprogramming of mouse skin fibroblasts from their library of 1,437 human transcription factors[46]. DLX4 was in their library, but was not included in the final screening. We could not obtain any ES-cell-like colonies from HDFs using the OSD cocktail. Conversely, we found that DLX4 promoted iPSC generation in HDFs only in the presence of KLF4. Therefore, it is possible that ectopic expression of DLX4 alone did not improve reprogramming efficiency in HDFs. It was thus excluded from the candidate list in the previous study.

Here we showed that the OS cocktail converted DP31 into a pluripotent state, although cells isolated from mature teeth (DP75) failed to be reprogrammed. This result indicates that DPCs isolated from immature teeth have unique properties. In this study, we have revealed that ectopic expression of DLX4 significantly promotes human iPSC generation; accordingly high expression levels of DLX4 in immature teeth DPCs are helpful for their effective reprogramming. Our results suggest that DLX4 plays a crucial role during reprogramming of DPCs and controls their reprogramming efficiency. However, the regulation of reprograming efficiency by DLX4 does not fully explain the unique properties of immature teeth DPCs. For example, the OSD cocktail was still insufficient to convert DP75 to a pluripotent state, conversely it up-regulated the reprogramming efficiency of DP31 to the same level provided by OSK. Moreover, DP87 shows substantially higher reprogramming efficiency but the expression level of DLX4 is average compared to other immature teeth DPC lines. This indicated that the measured endogenous DLX4 expression level determined by real-time PCR did not completely correlate with the reprogramming efficiency of DPCs and endogenous DLX4 expression may not be the sole factor responsible for the reprogramming efficiency to DPCs. A plausible explanation is that DLX4 may function together with some partner gene(s) to promote reprogramming, so the expression level of this (these) gene(s) may also affect the reprogramming efficiency of DPCs. Further screening of the genes listed in Supplemental Table S1 may lead to the discovery of additional factors that work together with DLX4.

An important remaining question is how DLX4 acts on a molecular level to promote reprogramming process in DPCs. Trinh et al. showed that DLX4 induces c-MYC and inhibits TGF-β mediated induction of $p15^{Ink4B}$ and $p21^{WAF1/Cip1}$ expression by blocking the TGF-β/Smad signaling pathway in normal and malignant epithelial cell lines[47]. Blockage of TGF-β signaling leads to promotion of MET, which is critical initiating event during the derivation of iPSCs from mesenchymal cells[19,20]. In this study we also observed that enforced expression of DLX4 in DPCs caused modest up-regulation of CDH1, however compared to KLF4, the potential to induce CDH1 is very mild. It was initially speculated that DLX4 may promote reprogramming process by activating the endogenous expression of c-MYC, because we found that DLX4 can restore the reprogramming efficiencies of DPCs and HDFs in the absence of c-MYC. The close correlation between DLX4 and c-MYC also has been shown in other cell types, such as hematopoietic cells[48,49]. Contrary to our expectation, we could not observe the up-regulation of c-MYC after induction of DLX4 in DPCs. Similar to c-MYC, enforced expression of DLX4 also did not affect the transcript levels of CDK inhibitors, such as $p21^{WAF1/Cip1}$, $p15^{Ink4B}$, and $p16^{Ink4A}$, which have been demonstrated as roadblocks against reprogramming[18,50–53]. On the other hand, we did observe that TGF- β suppressed the expression of DLX4 in DPCs and impaired iPSC generation. Although the TGF-β/activin signaling pathway is important for the maintenance of human embryonic stem cells[54,55], our results suggested that the TGF-β signaling associated with reduction of DLX4 is one of the roadblocks for effective reprogramming of human somatic cells. Since homeobox genes often function in a context dependent and lineage specific manner, the functions of DLX4 may be depended on the cell types. Although we have tested two mesenchymal linages of somatic cells whether DLX4 can promote reprogramming, it is desirable to test another cell types, such as epithelial and hematopoietic cells.

In this study we used conventional retroviral system to induce iPSCs and our process contains splitting step at 6 days post infection.

So we cannot formally exclude the possibility that we might count the ES-like colonies derived from the same clones and this could result in overestimation of reprogramming efficiencies. But as mentioned above, it was unlikely that DLX4 induced proliferation in DPCs before the splitting step and accordingly the number of ES-like colonies obtained from using DLX4 was increased.

Here we show that DPCs isolated from immature teeth are more easily reprogrammed into iPSCs than DPCs derived from adult teeth and identify *DLX4* as one of the candidate genes that is differentially expressed during the developmental stage. To our knowledge, this is the first report of a new transcript factor that enhances iPSC generation based on a comparative analysis of gene expression profiles using human cell resources. Our findings also provide evidence that our DPC collection obtained from many donors is a promising resource for both basic and clinical studies toward setting up a human iPS cell bank.

Methods

Cell culture. The isolation of DPCs was described in our previous report. DPCs were cultured in MSCGM (Lonza) and HDFs were cultured in DMEM with 10% FBS containing penicillin/streptomycin. The human ES cell line (KhES01) was obtained from Kyoto University and cultured on mitomycin C-treated SNL feeder cells in Primate ES cell medium (ReproCELL) supplemented with 4 ng/mL bFGF (WAKO). Human iPSCs were generated and maintained in the human ES cell culture condition.

Virus production and iPSC generation. We first introduced the mouse receptor for retroviruses (Slc7a1) into DPCs and HDFs using a lentiviral system according to our previous report[13,14]. Complementary DNA for human *OCT3/4, SOX2, KLF4,* and *c-MYC* was cloned into the retroviral pMXs vector, and *DLX4* was transferred to the pMXs-GW retroviral expression vector using the Gateway LR reaction. These pMXs-based retroviral vectors were separately transfected into Plat-E cells (ecotropic retrovirus packaging cells) using Fugene 6 (Roche). We also used a pMX retroviral vector encoding enhanced green fluorescent protein (*EGFP*) to monitor transduction efficiency by fluorescence-activated cell analysis (FACSAria, Beckton Dickinson). Twenty-four hours after transfection, the medium was replaced with fresh medium. After 24 hours, the viral supernatant was collected and mixed with an equal amount of each factor to infect HDFs/Slc7a1 and DPCs/Slc7a1 in medium supplemented with 4 μg/mL polybrene (Nacalai Tesque). Six days after retroviral infection, HDFs/Slc7a1 and DPCs/Slc7a1 were harvested by trypsinization and replated at 5×10^4 or 5×10^5 cells per 100-mm dish on mitomycin C-treated SNL feeder cells. The next day, the medium was replaced with primate ES cell medium supplemented with 4 ng/mL bFGF. Recombinant human TGF-β1 (reconstituted with 10 mM citric acid containing 0.1% BSA) was obtained from Pepro Tech. To evaluate the effect of activating TGF-β signal during reprogramming, we added TGF-β1 (5 ng/mL) into culture medium from day 1 to day 21 after retroviral infection, and counted the human ES-cell-like colonies obtained from 5×10^4 infected DPCs at day 21.

Assessment of reprogramming efficiency of DPC lines. To determine the reprogramming potential of DPCs isolated from various developmental stages, we introduced the *OSKM* transcription factors into nine DPC lines using a retroviral system. The generation of iPSCs was performed according to our general protocol. Since we found that the transduction efficiencies of DPCs are at similar levels in their early passages, we used DPCs within ten passages to induce iPSCs. We counted the human ES-cell-like colonies obtained from 5×10^4 infected DPCs at 21 days after infection. The assays were conducted three times. The number of the human ES-cell-like colonies obtained from each DPC line was normalized to the number obtained from DP31. The relative reprogramming efficiency of DP31 was set as 1.0.

Real-time PCR. Total RNA was isolated from the cells using an RNeasy Plus Mini Kit (Qiagen). Total RNA (500 ng) was used for the reverse transcription reaction with Rever Tra Ace-α (Toyobo) according to the manufacturer's instructions. For real-time PCR analysis, PCR amplification of cDNA was performed by using SYBR Premix Ex Taq (Takara) and analyzed using a Thermal Cycler Dice Real-Time System (Takara). Primer sequences are listed in Supplementary Table S2.

Immunofluorescence staining. The cells were fixed with 4% paraformaldehyde, and treated with PBS containing 5% normal goat or donkey serum, 1% BSA, and 0.2% TritonX-100. The following antibodies were used: SSEA3 (1 : 10), TRA-1-81 (1 : 50), TRA-1-60 (1 : 50) (these antibodies were used at Kyoto University and were kind gifts from Dr. Peter W. Andrews), anti-SSEA4, anti-TRA-1-81, anti-TRA-1-60 (1 : 500, all contained in the ES Cell Characterization Kit from Merck Millipore; these antibodies were used at Gifu University), anti-NANOG (1 : 20, R&D Systems), anti-OCT3/4 (1 : 1000, Santa Cruz Biotechnology), anti-βIII-tubulin (1 : 200, Cell Signal Technology), anti-βIII-tubulin (1 : 2000, Covance), anti-α-SMA (1 : 500, DAKO), and anti-AFP (1 : 100, R&D). Nuclei were stained using 1 μg/mL Hoechst33342 (Life Technologies).

EB formation and differentiation assay. For EB formation, we harvested iPSCs by treating them with collagenase IV. The clumps of cells were transferred to poly (2-hydroxyethyl methacrylate)-coated dishes containing DMEM/F12 supplemented with 20% knockout serum replacement (Life Technologies), 2 mM L-glutamine, 0.1 M non-essential amino acids, 0.1 M 2-mercaptoethanol (Life Technologies), and 0.5% penicillin/streptomycin. The medium was changed every other day. After eight days as floating cultures, EBs were transferred to gelatin-coated plates and cultured in the same medium for another eight days. Spontaneous germ-layer differentiation of EBs was assayed using markers for endoderm (AFP), mesoderm (α-SMA), and ectoderm (βIII-tubulin).

Teratoma formation. For teratoma formation, 3×10^5 iPSCs were injected into the testes of a SCID mouse using a Hamilton syringe. Nine weeks after injection, tumors were dissected and fixed with PBS containing 4% paraformaldehyde. After paraffin embedding, the tissue was sectioned and stained with hematoxylin and eosin.

DNA microarray. Total RNA was prepared using the RNeasy Midi Kit (Qiagen). RNA (250 ng) was converted to cDNA, amplified, and labeled with Cy3 using the Quick Amp Labeling Kit (Agilent). Labeled DNA was hybridized to a Whole Human Genome Microarray Kit, 4 × 44 K (Agilent) according to the manufacturer's protocol. After hybridization, the arrays were washed consecutively using a Gene Expression Wash Pack (Agilent) and scanned using the G2505C Microarray Scanner System (Agilent). The data were normalized and analyzed by using GeneSpringGX11 (Agilent). The level of gene expression was determined as the average difference, and we selected genes with at least a five-fold difference in expression between DPCs from immature teeth and those from mature teeth. The microarray data was submitted to the NCBI GEO database under the accession number (GSE52853).

Statistical analysis. The differences in mean values were assessed by using unpaired Student's t-test, with $P < 0.05$ considered statistically significant. Error bars indicate ± SD (n = 3).

1. Takahashi, K. *et al.* Induction of pluripotent stem cells from adult human fibroblasts by defined factors. *Cell* **131**, 861–872 (2007).
2. Yu, J. *et al.* Induced pluripotent stem cell lines derived from human somatic cells. *Science* **318**, 1917–1920 (2007).
3. Aasen, T. *et al.* Efficient and rapid generation of induced pluripotent stem cells from human keratinocytes. *Nat. Biotechnol.* **26**, 1276–1284 (2008).
4. Aoi, T. *et al.* Generation of pluripotent stem cells from adult mouse liver and stomach cells. *Science* **321**, 699–702 (2008).
5. Eminli, S., Utikal, J., Arnold, K., Jaenisch, R. & Hochedlinger, K. Reprogramming of neural progenitor cells into induced pluripotent stem cells in the absence of exogenous Sox2 expression. *Stem Cells* **26**, 2467–2474 (2008).
6. Hanna, J. *et al.* Direct reprogramming of terminally differentiated mature B lymphocytes to pluripotency. *Cell* **133**, 250–264 (2008).
7. Mali, P. *et al.* Improved efficiency and pace of generating induced pluripotent stem cells from human adult and fetal fibroblasts. *Stem Cells* **26**, 1998–2005 (2008).
8. Park, I. H. *et al.* Reprogramming of human somatic cells to pluripotency with defined factors. *Nature* **451**, 141–146 (2008).
9. Stadtfeld, M., Brennand, K. & Hochedlinger, K. Reprogramming of pancreatic beta cells into induced pluripotent stem cells. *Curr. Biol.* **18**, 890–894 (2008).
10. Haase, A. *et al.* Generation of induced pluripotent stem cells from human cord blood. *Cell Stem Cell* **5**, 434–441 (2009).
11. Loh, Y. H. *et al.* Generation of induced pluripotent stem cells from human blood. *Blood* **113**, 5476–5479 (2009).
12. Sun, N. *et al.* Feeder-free derivation of induced pluripotent stem cells from adult human adipose stem cells. *Proc. Natl. Acad. Sci. USA* **106**, 15720–15725 (2009).
13. Utikal, J., Maherali, N., Kulalert, W. & Hochedlinger, K. Sox2 is dispensable for the reprogramming of melanocytes and melanoma cells into induced pluripotent stem cells. *J. Cell Sci.* **122**, 3502–3510 (2009).
14. Tamaoki, N. *et al.* Dental pulp cells for induced pluripotent stem cell banking. *J. Dent. Res.* **89**, 773–778 (2010).
15. Giorgetti, A. *et al.* Generation of induced pluripotent stem cells from human cord blood using OCT4 and SOX2. *Cell Stem Cell* **5**, 353–357 (2009).
16. Kim, J. B. *et al.* Direct reprogramming of human neural stem cells by OCT4. *Nature* **461**, 649–643 (2009).
17. Stadtfeld, M., Maherali, N., Breault, D. T. & Hochedlinger, K. Defining molecular cornerstones during fibroblast to iPS cell reprogramming in mouse. *Cell Stem Cell* **2**, 230–240 (2008).
18. Banito, A. *et al.* Senescence impairs successful reprogramming to pluripotent stem cells. *Genes Dev.* **23**, 2134–2139 (2009).
19. Chen, T. *et al.* E-cadherin-mediated cell-cell contact is critical for induced pluripotent stem cell generation. *Stem Cells* **28**, 1315–1325 (2010).
20. Li, R. *et al.* A mesenchymal-to-epithelial transition initiates and is required for the nuclear reprogramming of mouse fibroblasts. *Cell Stem Cell* **7**, 51–63 (2010).
21. Ruiz, S. *et al.* A high proliferation rate is required for cell reprogramming and maintenance of human embryonic stem cell identity. *Current Biol.: CB* **21**, 45–52 (2011).
22. Kim, J. B. *et al.* Pluripotent stem cells induced from adult neural stem cells by reprogramming with two factors. *Nature* **454**, 646–650 (2008).

23. Eminli, S. *et al.* Differentiation stage determines potential of hematopoietic cells for reprogramming into induced pluripotent stem cells. *Nat. Genetics* **41**, 968–976 (2009).
24. Kim, J. B. *et al.* Oct4-induced pluripotency in adult neural stem cells. *Cell* **136**, 411–419 (2009).
25. Gronthos, S., Mankani, M., Brahim, J., Robey, P. G. & Shi, S. Postnatal human dental pulp stem cells (DPSCs) in vitro and in vivo. *Proc. Natl. Acad. Sci. USA* **97**, 13625–13630 (2000).
26. Gronthos, S. *et al.* Stem cell properties of human dental pulp stem cells. *J Dent Res* **81**, 531–535 (2002).
27. Stevens, A. *et al.* Human dental pulp stem cells differentiate into neural crest-derived melanocytes and have label-retaining and sphere-forming abilities. *Stem Cells Dev.* **17**, 1175–1184 (2008).
28. Takeda, T. *et al.* Characterization of dental pulp stem cells of human tooth germs. *J. Dent. Res.* **87**, 676–681 (2008).
29. Zhang, W. *et al.* In vivo evaluation of human dental pulp stem cells differentiated towards multiple lineages. *J. Tissue Eng. Regen. Med.* **2**, 117–125 (2008).
30. Chen, J. *et al.* BMPs functionally replace Klf4 and support efficient reprogramming of mouse fibroblasts by Oct4 alone. *Cell Res.* **21**, 205–212 (2011).
31. Ichida, J. K. *et al.* A small-molecule inhibitor of tgf-Beta signaling replaces sox2 in reprogramming by inducing nanog. *Cell Stem Cell* **5**, 491–503 (2009).
32. Lin, T. *et al.* A chemical platform for improved induction of human iPSCs. *Nat. Methods* **6**, 805–808 (2009).
33. Maherali, N. & Hochedlinger, K. Tgfbeta signal inhibition cooperates in the induction of iPSCs and replaces Sox2 and cMyc. *Curr Biol: CB* **19**, 1718–1723 (2009).
34. Datto, M. B., Yu, Y. & Wang, X. F. Functional analysis of the transforming growth factor beta responsive elements in the WAF1/Cip1/p21 promoter. *J. Biol. Chem.* **270**, 28623–28628 (1995).
35. Reynisdottir, I., Polyak, K., Iavarone, A. & Massague, J. Kip/Cip and Ink4 Cdk inhibitors cooperate to induce cell cycle arrest in response to TGF-beta. *Genes Dev* **9**, 1831–1845 (1995).
36. Merlo, G. R. *et al.* Multiple functions of Dlx genes. *Int. J. Dev. Biol.* **44**, 619–626 (2000).
37. Panganiban, G. & Rubenstein, J. L. Developmental functions of the Distal-less/Dlx homeobox genes. *Development* **129**, 4371–4386 (2002).
38. Morasso, M. I. & Radoja, N. Dlx genes, p63, and ectodermal dysplasias. *Birth Defects Res. Part C, Embryo Today: Rev.* **75**, 163–171 (2005).
39. Thomas, B. L. *et al.* Role of Dlx-1 and Dlx-2 genes in patterning of the murine dentition. *Development* **124**, 4811–4818 (1997).
40. Depew, M. J., Lufkin, T. & Rubenstein, J. L. Specification of jaw subdivisions by Dlx genes. *Science* **298**, 381–385 (2002).
41. Robledo, R. F., Rajan, L., Li, X. & Lufkin, T. The Dlx5 and Dlx6 homeobox genes are essential for craniofacial, axial, and appendicular skeletal development. *Genes Dev.* **16**, 1089–1101 (2002).
42. Heude, E. *et al.* Jaw muscularization requires Dlx expression by cranial neural crest cells. *Proc. Natl. Acad. Sci. USA* **107**, 11441–11446 (2010).
43. Chai, Y. *et al.* Fate of the mammalian cranial neural crest during tooth and mandibular morphogenesis. *Development* **127**, 1671–1679 (2000).
44. Duverger, O. *et al.* Neural crest deletion of Dlx3 leads to major dentin defects through down-regulation of Dspp. *J. Biol. Chem.* **287**, 12230–12240 (2012).
45. Price, J. A., Bowden, D. W., Wright, J. T., Pettenati, M. J. & Hart, T. C. Identification of a mutation in DLX3 associated with tricho-dento-osseous (TDO) syndrome. *Human Mol. Genetics* **7**, 563–569 (1998).
46. Maekawa, M. *et al.* Direct reprogramming of somatic cells is promoted by maternal transcription factor Glis1. *Nature* **474**, 225–229 (2011).
47. Trinh, B. Q., Barengo, N. & Naora, H. Homeodomain protein DLX4 counteracts key transcriptional control mechanisms of the TGF-beta cytostatic program and blocks the antiproliferative effect of TGF-beta. *Oncogene* **30**, 2718–2729 (2011).
48. Shimamoto, T., Nakamura, S., Bollekens, J., Ruddle, F. H. & Takeshita, K. Inhibition of DLX-7 homeobox gene causes decreased expression of GATA-1 and c-myc genes and apoptosis. *Proc. Natl. Acad. Sci. USA* **94**, 3245–3249 (1997).
49. Awwad, R. T. *et al.* Overexpression of BP1, a homeobox gene, is associated with resistance to all-trans retinoic acid in acute promyelocytic leukemia cells. *Ann Hematol* **87**, 195–203 (2008).
50. Hong, H. *et al.* Suppression of induced pluripotent stem cell generation by the p53-p21 pathway. *Nature* **460**, 1132–1135 (2009).
51. Li, H. *et al.* The Ink4/Arf locus is a barrier for iPS cell reprogramming. *Nature* **460**, 1136–1139 (2009).
52. Utikal, J. *et al.* Immortalization eliminates a roadblock during cellular reprogramming into iPS cells. *Nature* **460**, 1145–1148 (2009).
53. Xu, Y. *et al.* Proliferation rate of somatic cells affects reprogramming efficiency. *J. Biol. Chem.* **288**, 9767–9778 (2013).
54. Jiang, J. & Ng, H. H. TGFbeta and SMADs talk to NANOG in human embryonic stem cells. *Cell stem cell* **3**, 127–128 (2008).
55. Xu, R. H. *et al.* NANOG is a direct target of TGFbeta/activin-mediated SMAD signaling in human ESCs. *Cell stem cell* **3**, 196–206 (2008).

Acknowledgments

We thank Y. Kawamura (AIST) for technical support for the DLX4 expression vector, T. Tanabe (CiRA) for technical support for the OS-induced iPSCs, and T. Ichisaka (CiRA) for technical support of teratoma assay. We also thank our laboratory members for their technical help and fruitful discussions. This work was supported by grants from the Ministry of Education, Culture, Sports, Science, and Technology of Japan and the JST Yamanaka iPS Cell Project.

Author contributions

N.T. performed and designed most of the experiments, analyzed the data, and wrote the manuscript. K.T. performed and designed the experiments for OS-induced iPSCs. H.A. and M.I. performed the characterization of iPSCs. K.I. and D.H. generated iPSCs from DPCs. T.K. performed the computer analyses of the DNA microarray data. N.C., A.I., T.K. and T.S. analyzed all data in this study. N.G. provided the retroviral expression clones. S.Y. supervised this study. K.T. conceived and supervised this study, designed the experiments, analyzed the data, and wrote and approved the manuscript.

Additional information

Accession codes: The microarray data were submitted to the NCBI GEO database under the accession number (GSE52853).

Supplementary information accompanies this paper at http://www.nature.com/scientificreports

Competing financial interests: The authors declare no competing financial interests.

How to cite this article: Tamaoki, N. *et al.* The homeobox gene *DLX4* promotes generation of human induced pluripotent stem cells. *Sci. Rep.* **4**, 7283; DOI:10.1038/srep07283 (2014).

Biomedical Research (Tokyo) 35 (1) 25-35, 2014

Detection of tumor-associated antigens in culture supernatants using autoantibodies in sera from patients with bladder cancer

Sho MINAMI[1], Ryo NAGASHIO[1, 2], Junpei UEDA[1], Kazumasa MATSUMOTO[4], Naoki GOSHIMA[5], Manabu HATTORI[1, 3], Kazuo HACHIMURA[2], Masatsugu IWAMURA[4], and Yuichi SATO[1, 2]

[1] Department of Applied Tumor Pathology, Graduate School of Medical Sciences, Departments of [2] Molecular Diagnosis, [3] Clinical Cytology, School of Allied Health Sciences and [4] Department of Urology, School of Medicine, Kitasato University, Kitasato1-15-1, Minami-ku, Sagamihara-shi, Kanagawa 252-0373, Japan and [5] National Institute of Advanced Industrial Science and Technology, 2-42 Aomi, Koto-ku, Tokyo 135-0064, Japan

(Received 26 November 2013; and accepted 9 December 2013)

ABSTRACT

Secreted proteins play essential roles in the process of tumorigenesis, and the analysis of tumor-secreted proteins has been suggested as a promising strategy for identifying cancer biomarkers. In this study, we performed proteomic analysis to identify proteins secreted from bladder cancer cell lines that are recognized by autoantibodies in sera from patients with bladder cancer. In addition, autoantibodies against the identified proteins were validated using a dot-blot array with sera from patients with bladder cancer and normal controls. As the results, we detected twenty-five and thirty-two immunoreactive spots in sera from patients with high- and low-grade bladder cancer, respectively. In addition, validation analysis revealed that serum IgG levels of anti-calreticulin and matrix metalloproteinase-2 (MMP2) autoantibodies were significantly higher in bladder cancer patients than in normal controls (both $P < 0.05$). Furthermore, the serum IgG level of anti-MMP2 autoantibody was significantly higher in patients with high- compared to low-grade bladder cancer ($P < 0.05$). On multivariate analysis, the serum IgG level of anti-MMP2 autoantibody was an independent predictor of cancer-specific survival ($P < 0.05$). Based on these findings, serum IgG levels of anti-calreticulin and MMP2 autoantibodies may be novel biomarker candidates for bladder cancer and its clinical outcome.

Bladder cancer (BC) is the 7th most common cancer in men and the 17th most common in women in the world. The incidence of BC has been increasing in Japan, and it was about 20 and 5 per 100,000 Japanese males and females in 2002 (22). Approximately 75–85% of BC are diagnosed as non-muscle-invasive bladder cancer (NMIBC) at the first diagnosis, and around 70% of cases present as pTa, 20% as pT1, and 10% as carcinoma *in situ* lesions (23). NMIBC has a tendency to recur (50–70%) and may progress (10–20%) to a higher grade and/or muscle-invasive BC in time, which might lead to high cancer-specific mortality (46).

The histological tumor grade is one of the clinical factors associated with outcomes of patients with NMIBC. High-grade NMIBC generally shows a more aggressive behavior than the low-grade form, and increases the risk of a poorer prognosis (3, 32). Due to the unfavorable prognosis associated with high-grade NMIBC, differential diagnosis between high- and low-grade NMIBC might be crucial for more appropriate follow-up and aggressive treatment. Cystoscopy and urine cytology are commonly used techniques for the diagnosis and surveillance of BC. Cystoscopy can identify most papillary and

Address correspondence to: Yuichi Sato, PhD, Department of Molecular Diagnostics, School of Allied Health Sciences, Kitasato University, 1-15-1 Kitasato, Minami-ku, Sagamihara, Kanagawa 252-0373, Japan
Tel: +81-42-778-8013, Fax: +81-42-778-9854
E-mail: yuichi@med.kitasato-u.ac.jp

solid lesions, but is markedly invasive to the patients, whereas urine cytology is limited by operator dependence and low sensitivity. For these reasons, some tumor markers have been investigated (*e.g.* BTAstat, NMP22), but their sensitivity and specificity are limited. Also, they are unable to predict the clinical outcome of BC patients (1, 42, 44). Therefore, one of the most important clinical challenges is the identification of novel biomarkers for aggressive NMIBC destined to recur and progress following initial treatment that can be used to predict the outcome of patients.

Proteins secreted from tumor cells reflect the various states of the tumor in real time and under specific conditions, and their expression patterns are different from normal cell components. Thus, proteins secreted into several body fluids, such as the serum, urine, cerebrospinal fluid, tears, and saliva from tumor cells and conditioned media of cultured tumor cells have been investigated. Approximately 20–25% of cellular proteins are secreted into extracellular spaces, and these proteins play important roles in differentiation, invasion, metastasis, angiogenesis, and the regulation of cell-to-cell and cell-to-extracellular matrix interactions (6, 40, 48). It has been suggested that tumor-secreting proteins are a promising source of diagnostic biomarkers in tumors (33).

Tumor-associated antigens released into the blood stream could induce a humoral immune response and generate autoantibodies (AAbs) (11). Interestingly, the immune response to such antigens generates marked biological amplification even though tumor-associated antigens are undetectable in sera in the early stage of tumorigenesis (19). Hundreds of tumor-associated antibodies have been identified, and the potential for using AAbs as a novel biomarker useful for cancer diagnosis has been discussed (17). Furthermore, recent studies based on AAb profiling of cancer patients have suggested that AAbs may not be only diagnostic but also prognostic biomarkers (24).

In this study, we performed two-dimensional gel electrophoresis (2-DE) combined with immunoblot analysis to identify tumor-associated secreted antigenic proteins that elicit a humoral response in sera from BC patients. By comparing immunoreactive patterns in sera from high- and low-grade BC patients, novel tumor markers associated with the histological grade were obtained. The identified proteins were further validated by dot-blot analysis with a large number of sera from patients with BC and normal controls. Moreover, the relationships between serum IgG levels of AAbs and clinicopathological factors of BC patients were also evaluated.

MATERIALS AND METHODS

Serum samples. Ninety-five serum samples from BC patients who had not received any therapy at Kitasato University Hospital were collected and stored at −80°C until use. The 2002 TNM and WHO classifications were used for determination of the pathological stage and histological grade of the tumor. Clinical characteristics of BC patients whose sera were collected are shown in Table 1. Thirty-five serum samples from healthy donors were also collected and used as a control. This study was approved by the Ethics Committee of Kitasato University School of Medicine. All patients were informed of the aim of the study and gave consent for the use of their samples.

Cell culture and sample preparation for proteomic analysis. The human bladder cancer cell lines TCCSUP, T24, 5637, and RT4 were purchased from the American Type Culture Collection (Manassas, VA, USA). These cell lines were grown in RPMI-1640 (SIGMA Aldrich Corp., St. Louis, MO, USA) supplemented with 10% fetal bovine serum (Biowest, Nuaillè, France), 100 units/mL of penicillin, and 100 μg/mL of streptomycin (Life Technologies Corp., Carlsbad, CA, USA) at 37°C in 5% CO_2 and 95% humidified air and harvested when they reached a confluency of 60–70%. Then, cells were washed 3 times with phosphate-buffered saline without divalent ions (PBS(−)), and additionally incubated with serum-free medium (Hybridoma-SFM; Life Technologies Corp.) for 48 h. The collected culture supernatants were subjected to serial centrifugation to remove cells at 200 × *g* for 20 min at room temperature (R/T) and cell debris at 2,000 × *g* for 30 min at 4°C, respectively. Forty milliliters of culture supernatants from each cell line was concentrated by ultrafiltration (Amicon Ultra-15 centrifugal filter units with a 30-kDa molecular weight cutoff membrane; Millipore Corp., Billerica, MA, USA), according to the manufacturer's instructions. The concentrated samples were precipitated and components interfering with 2-DE were removed with a 2-D Clean-up Kit (GE Healthcare Bio-Sciences Corp., Piscataway, NJ, USA), according to the manufacturer's instructions. Precipitated samples were solubilized in lysis buffer (7 M urea, 2 M thiourea, 2% 3-[(3-cholamidopropyl) dimethylammonio] propanesulfonic acid, 10 mM tris(2-carboxyethyl)-phosphine hydrochloride

Table 1 *Clinicopathological characteristics of bladder cancer patients*

Characteristics		Number of patients (n = 95)	(%)
Gender			
	Male	73	(77)
	Female	22	(33)
Age			
	Range	29–88	
	Median	71	
Stage			
	NMIBC	63	(66)
	MIBC	32	(44)
Histological grade			
	High	71	(75)
	Low	24	(25)
Carcinoma in situ			
	Negative	90	(95)
	Positive	5	(5)
Nodal status			
	N0	82	(86)
	N1, N2	13	(14)
Lymphovascular invasion			
	M0	90	(95)
	M1, M2	5	(5)

NMIBC: non-muscle-invasive bladder cancer, MIBC: muscle-invasive bladder cancer, High: bladder cancer with high grade, Low: bladder cancer with low grade.

(TCEP), 2.5% pH 3–10 pharmalyte (GE Healthcare Bio-Sciences Corp.), and one tablet of complete mini EDTA-free protease inhibitors (Roche Diagnostics, Mannheim, Germany) per 10 mL of solution) using an ultrasonic homogenizer (VP-050; TAITEC Co., Ltd., Saitama, Japan), and centrifuged at 20,000 × *g* for 30 min at 4°C. Finally, the protein concentration was quantified using Protein Assay Reagent (Bio-Rad Laboratories, Hercules, CA, USA).

Two-dimensional gel electrophoresis. 2-DE was performed according to our previous study (30). The first-dimensional agarose isoelectric focusing gel (75 mm in length and 2.5 mm in inner diameter) was made with single pharmalyte pH 3–10 (GE Healthcare Bio-Sciences Corp.). Thirty-five micrograms of each protein extracted from culture supernatants of four cell lines were equally mixed and applied to the cathodic end of the agarose isoelectric focusing gel, and loaded in stepwise voltages as follows: 100 V: 20 min, 300 V: 15 min, 500 V: 15 min, 700 V: 60 min, and 900 V: 150 min at 4°C. After fixation in 10% trichloroacetic acid and 5% sulfosalicylic acid for 3 min at R/T with mild shaking, agarose gels were placed in distilled water and washed 3 times for 15 min each at R/T. The agarose gel was equilibrated in equilibration buffer (0.06 M Tris-HCl (pH 6.8), 2% sodium dodecyl sulfate (SDS), 10% glycerol, 5% 2-mercaptoethanol, and 0.02% bromophenol blue (BPB)). Then, the agarose gel was placed on the top of the second-dimensional 10% polyacrylamide gel, and loaded with a constant current at 20 mA/ gel.

Immunoblotting. The separated proteins on 2-DE gels were transferred to polyvinylidene difluoride (PVDF) membranes (Millipore Corp.) overnight at R/T with a constant voltage at 10 V. After blocking with 0.5% casein for 60 min, the membranes were reacted with 20-times-diluted mixed sera of four NMIBC patients each with high- or low-grade BCs with 0.05% casein/TBST for 15 h at 4°C. The membranes were washed 3 times with Tris-buffered saline containing 0.1% tween20 (TBST) and reacted with 1,000-times-diluted horseradish peroxidase (HRP)-conjugated rabbit anti-human IgG antibody (DAKO, Glostrup, Denmark) with 0.05% casein/TBST for 30 min at R/T. After washing another 3 times with TBST, immunoreactive spots on the membrane were visualized with stable DAB solution (Life Technologies Corp.) for 15 min at R/T. The visualized images were digitized with a high-resolution scanner (GT-9800; Seiko Epson Corp., Tokyo, Japan).

Identification of proteins recognized by autoantibodies. For the identification of proteins recognized by autoantibodies, the separated proteins on 2-DE gels were stained by coomassie brilliant blue (CBB) (PhastGel Blue R; GE Healthcare Bio-Sciences Corp.) solution, and staining images were digitized with a high-resolution scanner. In order to match the immunoreactive spots on the membrane with protein spots on the gel, both digitized images were overlayed using Adobe photoshop software (version 7.0; Adobe Systems Inc., San Jose, CA, USA). The protein spots matched with the immunoreactive spots were manually excised from the gel and destained with 50% acetonitrile/50 mM NH_4HCO_3 until they became colorless. The pieces of gel were dehydrated with 100% acetonitrile and dried under vacuum conditions. They were then rehydrated in 10 μL of trypsin solution containing 10 ng/μL trypsin (Trypsin Gold, Mass Spectrometry Grade; Promega, Madison, WI, USA) for 45 min at 4°C and incubated for 24 h at 37°C with a minimum volume of trypsin solution and 7 μL of 25 mM NH_4HCO_3. After incubation, the digested tryptic peptide solutions were collected, and the gel was washed once with 7 μL of 5% trifluoroacetic acid/50% acetonitrile and washed solutions were collected in the same tube. They were then subjected to peptide mass fingerprint (PMF) and MS/MS analyses for protein identification. Finally, they were spotted on a Prespotted AnchorChip 96 Set for Proteomics (Bruker Daltonics, Bremen, Germany) and analyzed with MALDI-TOF/TOF-MS using Autoflex III (Bruker Daltonics) and FlexAnalysis software (version 3.0.96; Bruker Daltonics) according to the manufacturer's instructions. PMF spectra were acquired in the positive reflector mode in a mass range from 320 to 4,000 Da using the default parameters with the main parameters. The calibration of PMF spectra was carried out using the calibrant spots equipped with AnchorChip according to the manufacturer's recommendations. Irrelevant masses including matrix (855.09, 861.10, 877.10) and autodigested tryptic masses (842.51, 1,045.56, 2,211.05, 2,225.14, 2,283.20, 2,807.20) were automatically and manually excluded from the analysis. MS spectra derived from PMF analysis were further validated by MS/MS analysis. Some of the strongest peaks in each MS spectrum were selected as precursor ions, and MS/MS spectra were acquired in the positive LIFT mode using the default parameters with the main parameters. The PMF and MS/MS spectra were processed with FlexAnalysis and BioTools software (version 3.0.183; Bruker Daltonics). Furthermore, the combined spectrum data were connected with the MASCOT Server (version 2.3; Matrix Science, London, UK; www.matrixsciences.com) and database searches were run using the IPI human database (version 3.82; 92,104 sequencies; 36,547,220 residues, http://www.ebi.ac.uk/IPI/Databases.html) with the following parameters: enzyme specificity, trypsin; variable modification, oxidation with methionine, propionamide, and pyridylethyl with cysteine; maximum of one missed cleavage site; peptide mass tolerance of 100 ppm; MS/MS (fragment ion) tolerance of 0.8 Da. The Mascot score of a hit above 62 and $P > 0.05$ was set as the threshold for protein identification.

Dot-blot analysis. Based on the results of both the above proteomic approaches and database information from Uniprot (http://www.uniprot.org/), secreted proteins were selected. The recombinant proteins corresponding to identified proteins were synthesized with Gateway entry clones using an *in vitro* wheat germ cell-free protein synthesis system (15). The recombinant proteins were solubilized in lysis buffer (62.5 mM Tris-HCl (pH 6.8), 2% SDS, 10% glycerol, 5% 2-mercaptoethanol, 0.001% BPB, and 1 M phenylmethylsulfonyl fluoride) and spotted onto PVDF membranes using a micro-dot-blot array (Kakengeneqs Co., Ltd., Chiba, Japan). After blocking with Tris-buffered saline with 2% Tween20 for 60 min at R/T, the membranes were reacted with a 400-times dilution of each serum from patients with BC or healthy controls with 0.05% casein/TBST for 15 h at 4°C. The membranes were washed 3 times with TBST for 5 min each at R/T and reacted with 1,000-times diluted HRP-conjugated rabbit anti-human IgG (DAKO) with 0.05% casein/TBST for 30 min at R/T. After a further 3 washings with TBST for 5 min each, signals were developed using Immobilon Western Chemiluminescent HRP Substrate (Millipore Corp.). The signal intensities were analyzed using DotBlotChip System software (version 4.0; Dynacom Co., Ltd., Chiba, Japan). Each normalized signal was represented by the positive intensity minus the background intensity around the spot.

Statistical analysis. Significant differences between clinical characteristics and serum IgG levels of AAbs were tested using the Mann-Whitney *U*-test. The area under the curve (AUC) and best cut-off point were calculated employing receiver-operating characteristic curve (ROC) analysis. Cumulative survival rates of patients were determined using the Kaplan-Meier method, and the significance of survival differences between high and low serum IgG levels of

AAbs was tested using the log-rank test. Multivariate analysis was performed by employing the Cox proportional hazards regression model. A *P*-value of < 0.05 was used to determine the level of significance. All statistical analysis were performed using StatFlex software version 6.0 (Artech Co., Ltd., Osaka, Japan).

RESULTS

2-DE immunoblot analysis

The proteins extracted from culture supernatants of four BC cell lines were separated by 2-DE and transferred onto the PVDF membranes, and reacted with mixed sera of four patients each with high- or low-grade BCs. As the results, we detected a total of 138 immunoreactive spots, of which 25 and 32 were detected only in patients with high- or low-grade BCs, respectively. A total of 81 were detected in both groups (Fig. 1D).

Identification of proteins recognized by autoantibodies

The protein spots that matched immunoreactive spots on the membrane were excised from CBB-stained 2-DE gel (Fig. 1B, C) and underwent in-gel digestion and MALDI-TOF/TOF MS analysis. As the results, in 133 of the 138 (96%) immunoreactive spots, 61 proteins were identified. In 24 of 25 (96%) immunoreactive spots, 17 proteins were detected, and in 29 of 32 (90%) immunoreactive spots, 21 proteins were detected, in sera from high- or low-grade BC patients, respectively. Of these, 14 proteins were classified as "secreted protein" according to the Gene Ontology database (http://www.geneontology.org/) (Table 2).

Dot-blot analysis of autoantibodies against identified proteins

We synthesized 13 recombinant proteins using a wheat germ cell-free system except for a collagen alpha-1(VI) chain which we failed to synthesize (Table 2). Serum IgG levels of each AAb in 95 BC patients and 35 normal controls were investigated by dot-blot analysis with recombinant proteins. In the results of univariate analysis, the mean value (±SD) of serum IgG levels of anti-calreticulin and matrix metalloproteinase-2 (MMP2) AAbs were 14.0 ± 4.4 and 47.1 ± 9.7 in BC patients, and 9.9 ± 2.0 and 34.6 ± 5.1 in normal controls, respectively. All serum IgG levels of anti-calreticulin and MMP2 AAbs

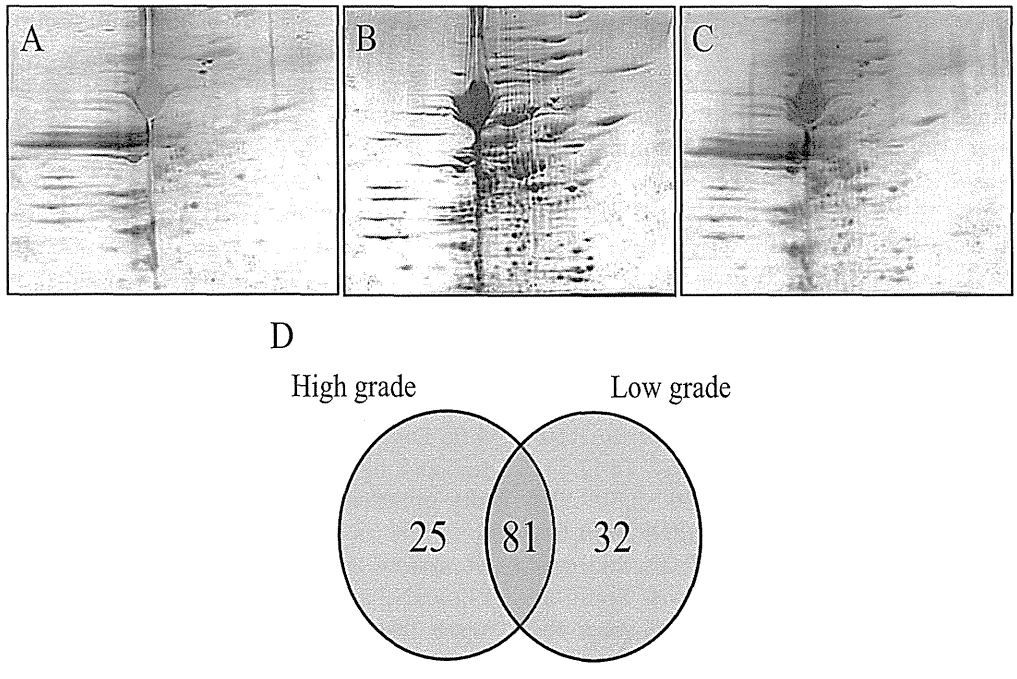

Fig. 1 Detection of autoantibodies by 2-DE immunoblot analysis in sera from BC patients. The proteins extracted from culture supernatants of the BC cell lines were separated by 2-DE and transferred to PVDF membranes. The membranes were incubated with mixed sera from BC patients (A). Protein patterns of CBB-stained 2-DE gel (B). Merged image of immunoreactive spots on the membranes and CBB-stained 2-DE gel (C). By comparing immunoreactive patterns, 25 and 32 spots were specifically detected in patients with high- and low-grade BC, respectively (D). The protein spots that matched immunoreactive ones on the 2-DE gel were excised and identified by MALDI-TOF/TOF MS.

Table 2 *Identified antigenic proteins in sera from high- or low-grade BC patients*

Gene symbol	Accession number	Protein name	Histological grade
CALR	P27797	Calreticulin	High
CTSD	P07339	Cathepsin D	High
SERPINB5	P36952	Serpin B5	High
MMP2	P08253	Matrix metalloproteinase-2	High
CPA4	Q9UI42	Carboxypeptidase A4	High
COL6A1	P12109	Collagen alpha-1(VI) chain	High
FBLN1	P23142	Fibulin-1	Low
MP10	P09238	Matrix metalloproteinase-10	Low
SPARC	P09486	SPARC	Low
MMP1	P03956	Matrix metalloproteinase-1	Low
CTSZ	Q9UBR2	Cathepsin Z	Low
SPON2	Q9BUD6	Spondin-2	Low
CTSL1	P07711	Cathepsin L1	Low
QSOX1	O00391	Sulfhydryl oxidase 1	Low

High: specifically detected in sera from high-grade BC patients.
Low: specifically detected in sera from low-grade BC patients.

were significantly higher in BC patients than in normal controls ($P < 0.01$, Fig. 2A, B). In addition, the mean value (±SD) of serum IgG levels of anti-calreticulin and MMP2 AAbs were 13.5 ± 3.1 and 40.4 ± 9.8 in the patients with low-grade BC, and 14.0 ± 4.6 and 66.3 ± 9.0 in those with high-grade BC, respectively. The serum IgG level of anti-MMP2 AAb was significantly higher in patients with high-grade than in low-grade BC ($P < 0.01$, Fig. 2D), but not for anti-calreticulin AAb (Fig. 2C). No significant difference in serum IgG levels of other AAbs between BC patients and normal controls was detected (data not shown).

Validation of anti-calreticulin and -MMP2 autoantibodies between BC patients and normal controls

Based on ROC analysis of anti-calreticulin AAb, an optimal cut-off value of 10.6 was applied, and the diagnostic sensitivity and specificity for BC patients were 64.0 and 60.0%, respectively. The AUC for anti-calreticulin AAb in BC patients compared to normal controls was 0.65 (95% confidence interval: 1.23–5.89, Fig. 3A). Regarding anti-MMP2 AAb, an optimal cut-off value of 34.6 was applied, and the diagnostic sensitivity and specificity for BC patients were 60.0 and 62.0%, respectively. The AUC for anti-MMP2 AAb in BC patients compared to normal controls was 0.59 (95% confidence interval: 0.73–3.45, Fig. 3B).

Association of serum IgG levels of anti-calreticulin and MMP2 autoantibodies with clinical outcomes

To estimate whether serum IgG levels of anti-calreticulin and MMP2 AAbs were of independent predictive value for recurrence-free survival or cancer specific-survival of BC patients, uni- and multivariate analyses were performed. At a median follow-up of 62.3 months (range: 2 to 166.4), Kaplan-Meier projection indicated that there was no significant correlation between the serum IgG level of anti-calreticulin AAb and recurrence-free or cancer-specific survival (Fig. 3C). However, the serum IgG level of anti-MMP2 AAb was significantly correlated with cancer-specific survival ($P < 0.05$; Fig. 3D). In addition, multivariate analysis with Cox proportional hazards regression analysis revealed that the serum IgG level of anti-MMP2 AAb and pathological stage were significantly correlated with cancer-specific survival ($P < 0.05$ each, Table 3). These findings suggest that an increased serum IgG level of anti-MMP2 AAb is an independent predictor of poorer survival in BC patients.

DISCUSSION

Secreted proteins reflect various states of cells in real time and under specific conditions, participate in various physiological processes, and play crucial roles in pathological processes. Thus, it has been suggested that the analysis of tumor-secreted proteins is a promising method to identify diagnostic biomarkers in cancer (6, 33, 40, 48). Actually, several studies have revealed that secreted proteins, which could be biomarker candidates, are present in the conditioned media of several tumor cells (25, 27, 47).

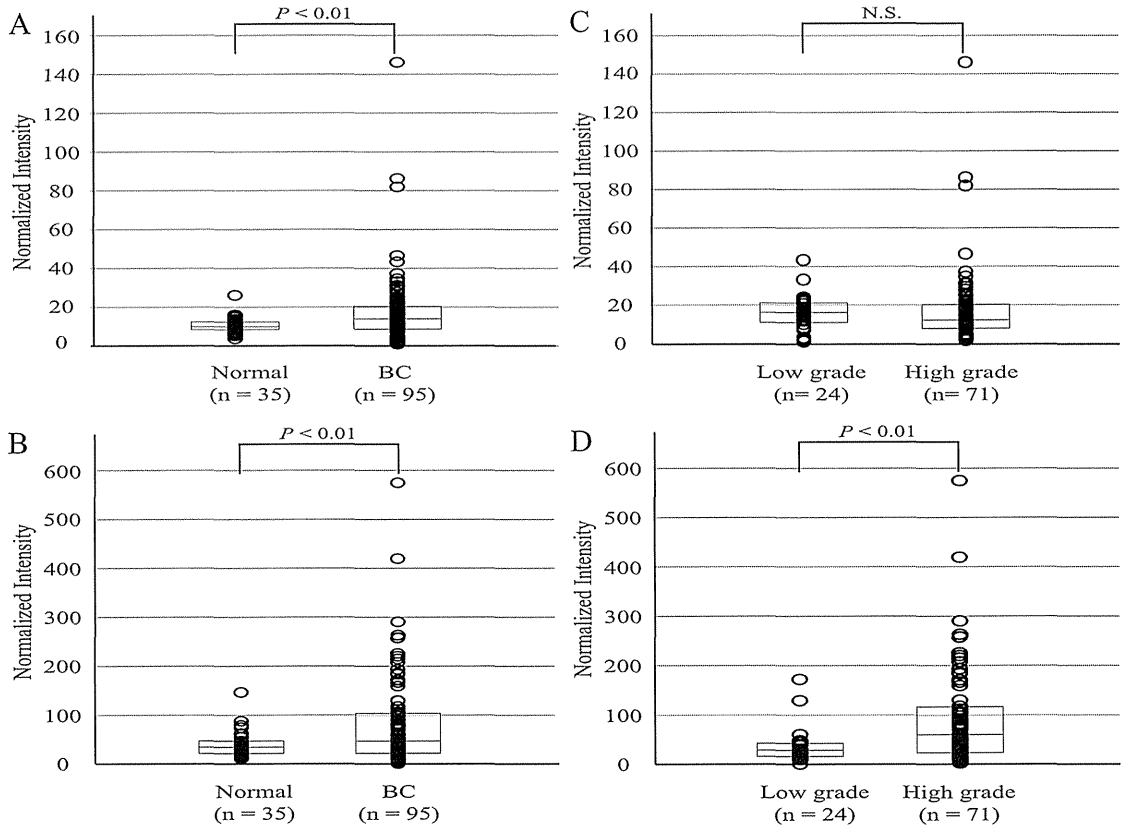

Fig. 2 Dot-blot analysis of serum IgG levels of anti-calreticulin and MMP2 AAbs. Serum IgG levels of anti-calreticulin and MMP2 AAbs in sera from BC patients and normal controls were detected by dot-blot analysis. The normalized intensity was calculated with the Mann-Whitney *U*-test. The serum IgG level of anti-calreticulin AAb was significantly higher in BC patients than in normal controls (A). No significant difference was detected between high- and low-grade tumors (C). The serum IgG level of anti-MMP2 AAb was significantly higher in BC patients than in normal controls (B) and significantly higher in high-grade than in low-grade BC patients (D). N.S.: not significant

AAbs against tumor-associated antigens have been identified in sera from patients with colon, breast, lung, ovary, and bladder cancers (4, 7, 16, 36, 50). Thus, the application of the humoral immune response for the detection of cancer biomarkers has a great potential and has been suggested as ideal screening for cancer diagnosis and their prognostic value (17, 24). Furthermore, the immune system is especially well adapted for the early detection of cancer, because AAbs can be detected before the appearance of other biomarkers or phenotypic alternations in an early stage of tumorigenesis (19).

Therefore, we performed 2-DE/immunoblot analysis to identify secreted antigenic proteins that are recognized by AAbs in the sera of BC patients. In this study, we picked up 57 immunoreactive spots that specifically differentiate the histological grade of BC. Furthermore, we confirmed the usefulness of identified AAbs as sero-diagnostic and/or -prognostic biomarkers for BC by dot-blot analysis. In the results, serum IgG levels of anti-calreticulin or MMP2 AAbs, which were identified in sera from patients with high-grade BC, were significantly higher in sera of BC patients than in normal controls. In addition, the serum IgG level of anti-MMP2 AAb was significantly correlated with the histological grade of the tumor and cancer-specific survival.

Calreticulin is diversely distributed in the cytoplasm, nucleus, plasma membrane, and extracellular spaces of cells. Because of these different localizations, it has been implicated in many cellular functions, including Ca^{2+} storage and signaling, lectin-like chaperoning, the regulation of gene expression, cell adhesion, migration, cellular proliferation, and autoimmunity (8, 26, 31). It has been reported that the overexpression of calreticulin was detected in tumor tissues and their sera of hepatocellular, colon, and lung cancers (18, 45, 49), and associated with the migration and proliferation of tumor cells and a poorer prognosis in esophageal, gastric, and breast